

Alma Mater Studiorum . Università di Bologna

DOTTORATO DI RICERCA IN

CHIMICA

Ciclo XXIX

Settore Concorsuale di afferenza: 03/B1

Settore Scientifico disciplinare: CHIM/03

**ORGANIC LIGHT-EMITTING TRANSISTOR AS AN EFFECTIVE
PHOTONIC DEVICE PLATFORM - SYSTEM
ENGINEERING FOR TUNING THE OPTOELECTRONIC
PERFORMANCE**

Presentata da: Emilia Benvenuti

Coordinatore Dottorato

Prof. Aldo Roda

Relatore

Prof. Alberto Credi

Correlatore

Dott. Stefano Toffanin

Esame finale anno 2017

Abstract

The increasing interest in organic electronics is connected with the easy processability and the possibility of molecular tailoring of the organic semiconductor materials. Ranging from dry deposition techniques in high vacuum to wet processes and nanopatterning techniques, small molecule and polymeric π -conjugated materials have been implemented in a plethora of optoelectronic device applications. Among the other, Organic Light-Emitting Transistors (OLETs) are emerging as an innovative class of multifunctional devices able to integrate the electronic properties of a transistor and the light generation capability.

In this thesis, we aim at investigating the photonic and optoelectronic performance of suitable-engineered devices based on different field-effect transistors architecture. Both the active layer and the gate dielectric layer of the device were investigated in order to increase the device performance in terms of brightness, color coordinate and external quantum efficiency. Starting from the study of the active layer in an ambipolar single-layer OLET, we succeeded in controlling the solid-state phases of the oligothiophene derivative bearing 2,3-thienoimide symmetric ends namely NT4N. By means of three different deposition techniques, i.e. thermal sublimation, supersonic molecular beam deposition and lithographically controlled wetting, we investigated the influence of the different molecular packing motifs on the field-effect charge mobility.

Given the limited number of efficient electroluminescent organic small molecules with high field-effect charge mobility, we adopted another approach for enhancing the figures of merit of OLET devices by implementing a multilayer heterostructure comprised by a charge-transport layer and a light-emitting layer in the OLET active region. By introducing a newly-synthesized anthracene-based twisted oligomer as emissive layer a deep blue emitting unipolar OLET was realized.

Finally, the integration of a high-capacitance hybrid photonic crystal as gate dielectric into the single-layer ambipolar OLET based on NT4N permitted to achieve low gate threshold voltages, and consequently intense brightness, together with as-designed modulation of the spectral and spatial characteristics of the emitted electroluminescence.

Contents

Introduction	1
Chapter 1	
Working principles and constituting elements in organic field-effect transistor devices	5
1.1 Introduction	5
1.2 Organic Field-Effect Transistor (OFET)	6
1.3 Organic Light-Emitting Transistors (OLETs)	8
1.4 OFETs/OLETs working principles	11
1.5 Key building blocks of OFETs/OLETs	16
Chapter 2	
Experimental setup	23
2.1 Thin-film deposition	23
2.2 Device fabrication	30
2.3 Thin-film characterization	31
2.4 Device optoelectronic characterization	32
Chapter 3	
Correlation between crystalline phase and field-effect charge transport in ambipolar small-molecule thin-films	35
3.1 Introduction	35
3.2 NT4N as active material in ambipolar single-layer OLETs	37
3.3 Processing-structure-function correlation in NT4N-based thin-films	39

3.4 Conclusions	51
-----------------	----

Chapter 4

Anthracene-based molecular emitters for non-doped deep-blue organic light emitting transistors

	55
4.1 Introduction	55
4.2 Synthesis	58
4.3 Optoelectronic properties of anthracene derivatives	58
4.4 Fabrication and characterization of unipolar bilayer OLET device	61
4.5 Conclusions	65

Chapter 5

Integration of multilayer high-k photonic crystal into transparent ambipolar OLET

	69
5.1 Introduction	69
5.2 Gate dielectric Photonic Crystal	71
5.3 Enhancement of optoelectronic performance in PhC-OLET	75
5.4 Modulation of optical characteristics in PhC-OLET	79
5.5 Conclusions	82

Conclusions

85

Introduction

Organic semiconducting materials constitute the active elements in new generations of plastic-optoelectronic devices ^[1]. These structures comprising molecular and polymeric units are characterized by π -conjugated bonds giving rise to delocalized filled and empty π -orbitals that greatly impact the optical and electrical properties ^[2]. Interest in organic electronics arise from the possibility to produce low-cost, large-area, light-weight and flexible devices able to integrate functionalities currently accomplished using more expensive conventional semiconductors and components ^[3]. Indeed, the main advantage of using organic materials is the easy processability. They can be deposited on virtually any substrates, including silicon backplanes and low-cost ones such as plastic, metal foils, and glass. Organic semiconductors can be processed by dry technique such as thermal sublimation in high and ultra high vacuum that ensure a high purity and molecular order in thin-film, but they are also compatible with wet deposition processes. Spin-coating deposition or ink-jet printing represent low-cost fabrication processes that can be implemented on large area, such as in roll-to roll fabrication technique ^[4]. Among the others, applications for organic semiconductors include organic thin-film transistors (OTFTs) ^[5], organic light-emitting diodes (OLEDs) ^[6] and transistors (OLETs) ^[7] and photovoltaic cells (OPVs) ^[8]. In particular, OLETs are highly integrated organic devices combining the light emission of OLEDs to the switching capability of a transistor and they can be considered as an intrinsically out-performing device for light generation and out-coupling ^[9].

To turn organic optoelectronic devices into a power-efficient light source, three key parameters must be addressed. The internal electroluminescence (EL) quantum efficiency must be close to one (high internal quantum efficiency) ^{[10][11]}, a high fraction of the internally created photons must escape to the forward hemisphere (high out-coupling efficiency) ^{[12][13]} and the energy loss during electronóphoton conversion should be small (low operating voltage) ^[14]. The potential application of OLETs in next-generation active-matrix display technology indeed demands precise requirements in term of brightness, external quantum efficiency (EQE) and colour coordinate.

In this thesis, we aim at engineering the OLET architecture by optimizing specifically the constituting elements such as the active layer and the dielectric layer in order to increase the optoelectronic figures of merit of the entire device platform. As a first step,

we implement the simplest OLET structure where a single-material active layer is capable of both electron and hole transport and light emission for investigating the correlation between thin-film structural and morphological features and the device optoelectronic performance. In order to probe the different crystalline phases and supramolecular arrangement configuration spanned by the small-molecule organic semiconductor in the device active layer, we implement different deposition techniques, both dry physical and liquid-based methods.

Indeed, it is well-known that the structure of the active layer has a strong impact on the functional properties, so understanding the structure formation, i.e. the growth process, and finding ways to optimize the molecular arrangement is a prerequisite for technological progress of the device platform^[15].

As a second step in our strategy, we introduce a multilayer stack in the active region of the OLET so that each layer comprising the stack may be optimized independently and according to a specific function. In particular, we aim at decoupling the charge carrier function from the electroluminescence capability: thus, we introduced a bilayer structure where a newly-synthesized anthracene derivative is deposited as single-component emission layer on top of a high-mobility hole-transport semiconductor. In this case, the external quantum efficiency and the CIE color coordinates are the key parameters to be enhanced in a blue emitting OLET.

In the case we aim at achieving high brightness in the transistor-based device, a typical route to pursue is to engineer the dielectric layer for lowering the operating voltage. In the approach we adopted we integrated a hybrid photonic structure as dielectric layer in order to increase the functional properties of the engineered OLET. Indeed, we succeeded in demonstrating a reduced threshold voltage in the device together with the possibility to modulate the electroluminescence features.

This thesis is developed as follows: in Chapter 1 a general description of the working principles and the constituting elements of organic field-effect transistor devices is presented. In Chapter 2 the experimental setups used to fabricate and characterize the thin-film field-effect transistor devices are described. In Chapter 3 the ambipolar and light-emitting oligothiophene derivative named NT4N is used as active material in a single-layer OLET. In particular, the correlation between processing method, solid-state packing/supramolecular arrangement and functional properties (i.e. charge mobility and electroluminescence) in NT4N prototypical linear conjugated compound is investigated

by implementing different deposition techniques such as thermal sublimation, Supersonic Molecular Beam Deposition and Lithographically Controlled Wetting. In Chapter 4 a new anthracene-based derivative compound is used as an efficient emission layer in multilayer OLET device for achieving deep-blue emission, and compared with different anthracene-based derivatives already reported in literature. Finally, in Chapter 5 an innovative strategy for obtaining a simultaneous increase in the device brightness together with a modulation of the spectral emission and spatial distribution of the device electroluminescence is implemented by integrating an oxide-based multilayer photonic crystal as a dielectric stack into a single-layer ambipolar OLET.

Reference

- [1] F. F. Vidor, T. Meyers, U. Hilleringmann, M. Jacob, *Electronics* **2015**, *4*, 480.
- [2] A. Facchetti, *Mater. Res.* **2007**, *10*, 28.
- [3] M. Muccini, *Nat. Mater.* **2006**, 605.
- [4] M. Muccini, S. Toffanin, *Organic Light-Emitting Transistors: Towards the Next Generation Display Technology*, Ed. Wiley-Science, Wise Co-Publication, **2016**.
- [5] J. Mei, Y. Diao, A. L. Appleton, L. Fang, Z. Bao, *J. Am. Chem. Soc.* **2013**, *135*, 6724.
- [6] J.-H. Jou, S. Kumar, A. Agrawal, T.-H. Li, S. Sahoo, *J. Mater. Chem. C* **2015**, *3*, 2974.
- [7] R. Capelli, S. Toffanin, G. Generali, H. Usta, A. Facchetti, M. Muccini, *Nat. Mater.* **2010**, *9*, 496.
- [8] N. Yeh, P. Yeh, *Renew. Sustain. Energy Rev.* **2013**, *21*, 421.
- [9] M. Melucci, L. Favaretto, M. Zambianchi, M. Durso, M. Gazzano, A. Zanelli, M. Monari, M. G. Lobello, F. De Angelis, V. Biondo, G. Generali, S. Troisi, W. Koopman, S. Toffanin, R. Capelli, M. Muccini, *Chem. Mater.* **2013**, *25*, 668.
- [10] B. H. Sasabe, J. Takamatsu, T. Motoyama, S. Watanabe, G. Wagenblast, N. Langer, O. Molt, E. Fuchs, C. Lennartz, *Adv. Mater.* **2010**, *22*, 5003.
- [11] H. Uoyama, K. Goushi, K. Shizu, H. Nomura, C. Adachi, *Nature* **2012**, *492*, 234.
- [12] Z. B. Wang, M. G. Helander, J. Qiu, D. P.uzzo, M. T. Greiner, Z. M. Hudson, S. Wang, Z. W. Liu, Z. H. Lu, *Nat. Photonics* **2011**, *5*, 753.
- [13] K. Leo, S. Reineke, F. Lindner, G. Schwartz, N. Seidler, K. Walzer, *Nature* **2009**,

459, 234.

- [14] J. Liu, H. Zhang, H. Dong, L. Meng, L. Jiang, L. Jiang, Y. Wang, J. Yu, Y. Sun, W. Hu, A. J. Heeger, *Nat. Commun.* **2015**, *6*, 1.
- [15] F. Schreiber, *Phys. Status Solidi* **2004**, *201*, 1037.

Chapter 1

Working principles and constituting elements in organic field-effect transistor devices

1.1 Introduction

Organic materials with a π -conjugated (hetero)aromatic backbone are capable of transporting charge and interact efficiently with light. Therefore, these systems can act as semiconductors in optoelectronic devices similar to inorganic materials ^[1]. However, organic semiconductors exhibit structural versatility, that is the possibility to tune their functional properties by the molecular design opening new possibilities for inexpensive device manufacturing ^[2]. In contrast to inorganic semiconductors, the solid-state structure of these materials is based on weak interactions, principally van der Waals and dipole-dipole interactions, between neighboring molecules/polymer providing realizations of systems in which transport is intermediate between conventional low-mobility hopping transport in amorphous glasses and high-mobility band transport in covalently bonded single-crystals ^[3]. Charge transport in solid involves electron transfer between molecules or molecular chains but to date the exact nature of charge transport in organic semiconductors is still open to debate. Nevertheless, it is possible to make a clear distinction between disordered semiconductors such as amorphous polymers and highly ordered organic single crystals, at the opposite ends of the spectrum. Charge transport in disordered semiconductors is generally described by thermally activated hopping of charges through a distribution of localized states or shallow traps. In the case of highly ordered molecular crystals, such as rubrene, tetracene, and pentacene, experimental data seem suggest band-like transport in delocalized states instead of

hopping transport. A common building block for the modeling of disordered semiconductors and highly ordered organic single crystals is the transfer integral representing the electronic coupling of adjacent molecules and the polaronic relaxation energy, which is the energy gained when a charge geometrically relaxes over a single molecule or polymer segment. This is an important parameter, which determines the probability of charge transport from one molecule to another and depends strongly on the particular molecule and the relative position of the interacting units ^[4].

To date, great number of π -conjugated semiconducting materials have been synthesized for use as active layers in organic electronics and important relations between molecular structure and structural organization in the solid state, film morphology, and, ultimately, electrical performance have been drawn ^{[5][1]}.

1.2 Organic Field-Effect Transistor (OFET)

A transistor is a semiconductor device commonly used as an amplifier or an electrically controlled switch. Since their discovery, transistors have been widely exploited in microelectronics industry as the fundamental building blocks for basic analytical circuits. An Organic Field-Effect Transistor (OFET) is a transistor based on organic semiconductors. The first OFET was reported by A. Tsumara in 1986 ^[6]. To date, significant improvements have been reached in materials performance and development of new fabrication techniques. OFETs are technologically attractive because all their layers can be deposited at low temperature and with low cost, in a large area and on a flexible substrate ^[7]. With the transistor performance that is readily available today a wide range of applications can already be addressed, in particular, e-paper displays, simple circuits ^[8], and chemical and biological sensors ^[9].

Nevertheless, because conjugated organic solids are more like insulators than semiconductors, charge transport in these materials is much less efficient than in conventional semiconductors. The problem is more crucial in transistors, where charges have to travel along much longer ways than in diodes. At the current state-of-the-art, mobility in organic thin-film transistor ranges between 0.01 and 10 $\text{cm}^2\text{V}^{-1}\text{s}^{-1}$, which is still much lower than what found in inorganic semiconductors (mobility is around 1000 $\text{cm}^2\text{V}^{-1}\text{s}^{-1}$ in silicon) ^[10]. In order to make these devices more suitable for various applications an important step is to increase the charge carriers mobility. Charge-carrier

mobility is the most important feature characterizing charge transport ability and is defined as the ratio between the charge drift velocity and the driving electric field.

The main constituting elements of an OFET are: three contacts (source, drain and gate), an active semiconducting material and a dielectric layer (Figure 1.1). These key elements can be combined to obtain different device structures. According to the adopted device configuration, OFETs can be divided into: top contact/bottom gate (TC/BG), top contact/top gate (TC/TG), bottom contact/top gate (BC/TG), bottom contact/bottom gate (BC/BG) ^[10].

The active part of the device is constituted of an organic semiconductor thin film equipped with two electrodes: the source and the drain. The distance between the source and the drain is called the channel length L while the transverse dimension of the structure is the channel width W . A third electrode, the gate, is laid out along the channel between the source and the drain; this electrode is electrically isolated from the semiconductor film by a thin insulating film, hence forming a metal-insulator-organic semiconductor (MIS) structure.

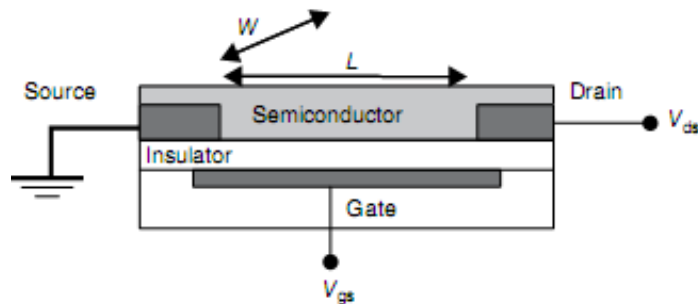


Figure 1.1 Schematic structure of a field-effect transistor and applied voltages: L , channel length; W , channel width; V_{ds} , drain voltage; V_g , gate voltage; V_t , threshold voltage; and I_{ds} , drain current ^[10].

Voltage is usually applied to the gate electrode (V_g) and between drain and source electrodes (V_{ds}). The source electrode is normally grounded ($V_s=0$). The dielectric is sandwiched between the gate and the organic semiconductor, and they work as two plates of a plane capacitor. Thus, when a gate voltage is applied, charges of different sign are accumulated at gate/dielectric and dielectric/organic semiconductor interfaces. The number of accumulated charges is proportional to V_g and the capacitance C_i of the insulator. Much of this accumulated charge in the active material is mobile and moves in response to the applied voltage between the other two electrodes, source and drain.

When no V_g is applied there are ideally no free charge carriers, and the device is off. Otherwise, with applied V_g the device is on (in real device a minimum gate voltage, the threshold voltage, has to be applied in order to overcome traps present in the film). This gate-induced charge carrier creation is called field-effect, and it is the key-idea of the working principle of FETs ^[11].

When incorporating the organic semiconductors into field-effect transistor configurations to evaluate their charge-transport characteristics in combination with a specific gate dielectric, many of these materials exhibit hole accumulation behavior for negative applied gate voltages. However, when the gate voltage polarity is reversed to positive values, the formation of an electron accumulation layer is much less commonly observed. For many organic semiconductor-based FETs, only p-channel operation seems possible. For this reason, such materials have been called "p-type" organic semiconductors. The realization of "n-type" OFETs usually involved the synthesis of special organic semiconductors with high electron affinities. In recent years, it has become clear that the chemical structure of the organic semiconductor is not the only factor that determines whether an OFET exhibits predominantly p-channel or n-channel behavior. Processing conditions, device architecture, and choice of electrodes are important as well ^[4]. A key discovery was the identification of the crucial role of the gate dielectric and in particular the identification of electron trapping mechanisms at the interface between the organic semiconductor and dielectric layers. This subsequently led to the general observation of n-channel and ambipolar characteristics in a broad range of polymer semiconductor FETs based on trap-free gate dielectrics ^[12]. This evidence suggested that organic semiconductors are intrinsically ambipolar and thus capable of conducting both electrons and holes in suitable device configurations and under inert testing conditions ^[13].

1.3 Organic Light-Emitting Transistors (OLETs)

The development of ambipolar OFETs offers not only new possibilities for complementary logic circuit design, but also the potential to control electron-hole recombination to afford light emission if the active material is also capable of electroluminescence. Organic Light-Emitting Transistors (OLETs) are devices able to combine the electrical switching capability of a field-effect transistor with the capability

of light generation. Excitons are thus created by the recombination of in-plane moving electron- and hole-currents, which are controlled by the gate electrode. OLETs are particularly interesting because they present charge carriers densities higher compared to Organic Light-emitting Diodes (OLEDs) ^[14]. Moreover, OLET configuration gives the possibility to reduce the exciton quenching with the metal electrode and prevent exciton-charge quenching thus leading to a higher electroluminescence quantum efficiency with respect to the standard sandwich configuration of an OLED. They also offer a convenient planar structure for investigating recombination physics in organic semiconductors using spatially resolving probes ^[15].

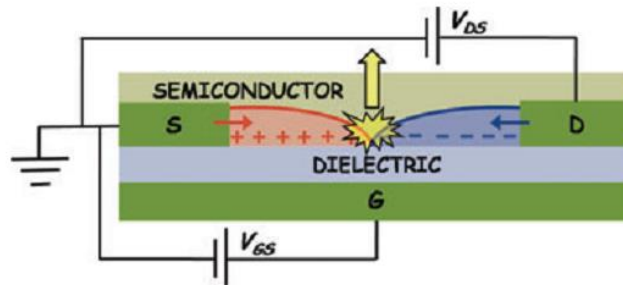


Figure 1.2 Schematic of an organic light-emitting field-effect transistor. By applying the suitable potential V_{ds} between drain (D) and source (S) and V_{gs} between gate (G) and source simultaneous injection in the channel of holes and electrons is possible. Charge recombine within the channel in a position controlled by the gate voltage ^[16].

Organic semiconductors are ideal candidates for light-emission applications since many small-molecule and conjugated polymer semiconductors show very high photoluminescence (PL) and electroluminescence (EL) efficiencies over the whole visible spectrum as well as decent charge transport properties, which enable their use in light-emitting device ^[4]. The first light-emitting transistor based on an organic semiconductor was reported in 2003 by Hepp et al. ^[17] in a single-layer unipolar tetracene based device. Surprisingly, despite the electrical unipolar charge behavior they observed light emission from tetracene. In unipolar OLET, charges of only one sign are transported along the channel, and the EL emission is localized in a narrow region in the proximity of the electrode that injects the minority carriers (electron tunneling from the metal work-function level to the lowest unoccupied molecular orbital (LUMO) level of tetracene has been proposed ^[18]). However, most of the scientific and technological characteristics that make light-emitting transistors attractive are only present in

ambipolar OLETs. They can be composed by a single organic semiconductor capable of transporting both electrons and holes (single-layer configuration) or by a combination of two unipolar transport materials in a vertical stack (bilayer configuration) ^[19]. Recently, the single-layer-and bilayer-based organic structures have been replaced by a trilayer stack consisting of an emission layer sandwiched between an electron- and a hole-transporting layer. The use of a multilayer architecture, where each layer can be optimized according to its specific function (charge transport, energy transfer, radiative exciton recombination) led to an external quantum efficiency of 5 % that outperforms the corresponding OLEDs based on the same emitting layer and optimized transport layers ^[20]. Indeed it is very challenging finding a single material capable of providing both high current density and intense electroluminescence in single-layer field-effect device given that these characteristics typically exclude one another in the solid state ^[21]. Other strategies can be implemented for improving brightness in OLETs such as the introduction of photonic structures in order to engineer the overall device architecture for optimizing light-extraction and out-coupling. The use of microcavity and photonic crystals in OLEDs was demonstrated to modify the extracted light emission ^[22]. This approach can also be implemented in OLETs for improving the device brightness by inserting the photonic structure in the gate dielectric, which becomes in this way optically active ^[23]. Indeed, the high-refractive-index and light-absorbing materials, such as doped Si and ITO, which are used to fabricate the gate electrode, introduce waveguiding effect and loss channels for the generated electroluminescence. Therefore, the interface between the dielectric and the active layer can be optically engineered by introducing a gate dielectric capable of reflecting light, which would be otherwise lost, to increase the device light output^[13].

In terms of applications, OLETs may constitute a key element for the development of next-generation organic active matrix display technology. Indeed, OLETs offer the possibility to combine the electrical properties of a transistor with light-emitting capability in a single device function, thereby reducing in principle the complexity of next generation pixel circuitry ^[24].

1.4 OFETs/OLETs working principles

A clear overview of the fundamental physics of OFETs can be found in literature [11][4][25]. In particular, the working principles of unipolar and ambipolar OFETs that are reported here are described according to [13].

Unipolar OFET/OLET working principle

An n-channel OFET (i.e., electrons are transported through the channel) can be used as an example to understand the basic device operational regimes due to the gate voltage dependence of the distribution of free charges in the active material. Real devices are far from being ideal and not all induced charges are mobile; a large number of deep charge traps are present in the film (deep enough to effectively immobilize electrons trapped in them). Deep traps have to be filled before the additionally induced charge can move. Thus, a minimum gate voltage has to be applied to obtain free electron density in the channel, the threshold voltage, V_t . Obviously, in n-channel OFETs V_t is higher than zero (for a p-channel OFETs, V_t is lower than zero since the charges flowing are positive).

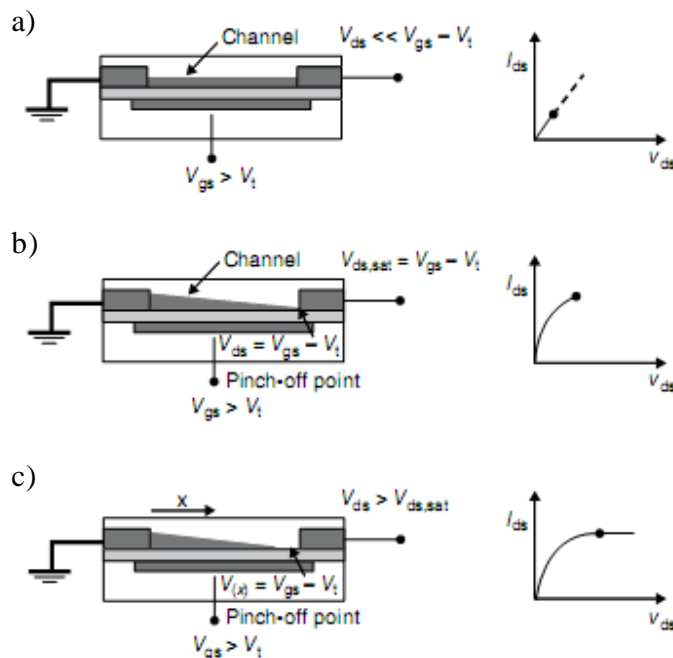


Figure 1.3 (a) Schematic structure of a field-effect transistor and applied voltages: L , channel length; W , channel width; V_{ds} , drain voltage; V_{gs} , gate voltage; V_t , threshold voltage; and I_{ds} , drain current. (b) Illustrations of operating regimes of field-effect transistors: (b) linear regime; (c) start of saturation regime at pinch-off; (d) saturation regime and corresponding current-voltage characteristics [4].

When no source-drain bias is applied, the charge-carrier concentration in the transistor channel is uniform. When a small source-drain voltage is applied ($V_{ds} \ll V_g - V_t$, Figure 1.3 a) a linear gradient of charge density is formed. The potential $V(x)$ within the channel increases linearly from the source ($x = 0$, $V(x) = 0$) to V_{ds} at the drain electrode ($x = L$, $V(x) = V_{ds}$). This is the linear regime in which the current flowing through the channel is directly proportional to V_{ds} . When the source-drain voltage is further increased, a voltage potential value $V_{ds} = V_g - V_t$ is reached, at which the channel is "pinched off" (Figure 1.3 b). That means a depletion region forms next to the drain because the difference between the local potential $V(x)$ and the gate voltage is now below the threshold voltage. A space-charge-limited saturation current I_{ds} , can flow across this narrow depletion zone as carriers are swept from the pinch-off point to the drain by the comparatively high electric field in the depletion region. Further increasing the source-drain voltage will not substantially increase the current but leads to an expansion of the depletion region and thus a slight shortening of the channel. Since the potential at the pinch-off point remains $V_g - V_t$ and thus the potential drop between that point and the source electrode maintains constant, the current saturates at a level I_{ds}^{sat} (Figure 1.3 c). The current-voltage characteristics in the different operating regimes of an OFET can be described analytically, in a simplistic way assuming that (i) the transverse electric field induced by the gate voltage is largely higher than the longitudinal field induced by the gate bias (gradual channel approximation) and (ii) the mobility is constant all over the channel. Assumption (i) is justified by the geometry of the device since the distance from the source to the drain is often much larger than the thickness of the insulator. Assumption (ii) is almost always fulfilled in inorganic semiconductors, while is only true at a first approximation in real organic semiconductors. In short, I-V characteristics can be drawn by either varying the drain voltage at a constant gate voltage (output characteristics) or changing the gate voltage at a fixed drain voltage (transfer characteristics). Locus characteristics are obtained by varying simultaneously drain voltage and gate voltage and keeping them at the same value. In the output characteristics, the curves are divided into a linear regime at low V_{ds} that turns into the saturation regime when $V_{ds} > V_g - V_t$. The current I_{ds} in both regimes is given by the equations:

$$I_{ds}^{lin} = \frac{W}{L} C_i \mu \left[(V_g - V_t) V_{ds} - \frac{V_{ds}^2}{2} \right]$$

$$I_{ds}^{sat} = \frac{W}{2L} C_i \mu (V_g - V_t)^2$$

where C_i is the capacitance of the dielectric per unit area (F/m^2) and μ is the charge carrier mobility.

A widely used method for parameter extraction from the characteristics curve consists in plotting the square root of the saturation current as a function of gate voltage. As it is clear from the saturation-regime curve, the square root of the saturation regime is supposed to give a straight line whose slope is an estimation of the mobility while its extrapolation to the x axis corresponds to the threshold voltage.

Ambipolar OFET/OLET working principle

The ambipolar condition can be obtained either by intrinsic properties of the organic semiconductors, or by superimposing organic semiconductors of opposite charge carriers or by blending of two opposite charge organic semiconductors. The mathematical description of the ambipolar curves is the same for the three cases, but the interpretation of the device main parameters must take in account the charge injection, charge accumulation and charge recombination processes that depend on the specific device structure.

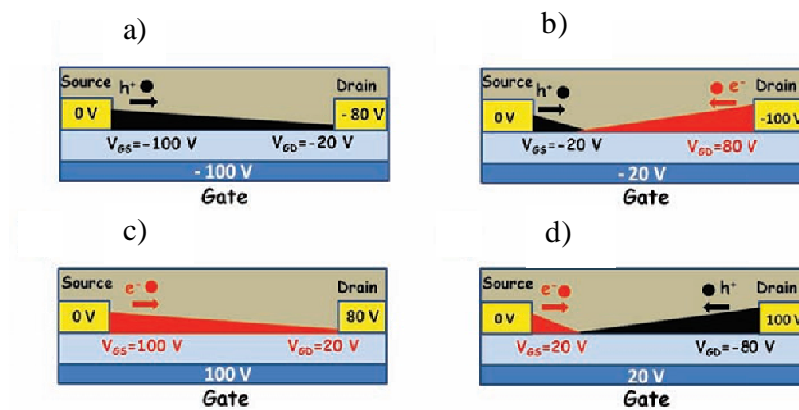


Figure 1.4 Example of an ambipolar OFET working in unipolar regime biased for hole transport (a) or electron transport (b). In this cases the V_{gs} and V_{gd} have the same sign. In ambipolar regime, instead, there are two more cases, (c) when gate is p-type (negative) polarized and (d) when gate is n-type (positive) polarized. These regimes are characterized by V_{gs} and V_{gd} of opposite signs.

In an ambipolar transistors, both holes and electrons are simultaneously injected in the channel by the source and drain electrodes, when they are biased at a suitable voltage. This voltage has to be higher in absolute value with respect to the hole and electron gate threshold voltages. Let us assume a transistor at a given positive drain voltage V_{ds} and start with a positive gate voltage of $V_{gs} = V_{ds}$. Just as in a unipolar transistor, the gate is more positive than the source electrode, and thus, electrons are injected from the source into the accumulation layer and drift toward the drain, given that $V_{ds} > V_t^e$ with V_t^e the threshold voltage for electron accumulation. Only one polarity of charge carriers is present, and ambipolar OFET is said to be working in unipolar region. When V_{gs} is smaller than V_{ds} , the gate potential is more negative than that of the drain electrode by $V_{gs} \leq V_{ds}$. While, the source will not inject electrons given $V_{gs} < V_t^e$, the drain electrode in an ambipolar transistor will inject holes into the channel if $V_{gs} \leq V_{ds} < V_t^h$, where V_t^h is the threshold voltage for hole accumulation. Thus, a hole current will flow and the measured I_{ds} current is increased differently from the case of unipolar n-channel transistor that would be now in an off state. If the two conditions on V_{gs} are simultaneously fulfilled, such as $V_{gs} > V_t^e$ and $V_{gs} \leq V_{ds} < V_t^h$, both electrons and holes are present in the channel. This regime is called the ambipolar regime, in contrast to the unipolar regime, where only charges with only one polarity are present in the channel for any particular biasing conditions. In a typical ambipolar OFET, the electrical curves show characteristic curves not displayed by unipolar devices. In the $I \text{ vs } V$ transfer curves in the saturation regime, instead the behavior of an ideal ambipolar OFET is represented by a typical V-shaped curve. Each branch of the curve represents a different charge carrier. For gate voltage values in the proximity of the edges of the curve, there is a unipolar I_{ds} current whose charge carrier type is defined by the local difference of applied voltages at the source, drain, and gate electrodes. The drain-source current minimum (so that, the bottom of the V-shaped curve) is reached when the two charge-carriers currents are balanced (maximum of ambipolar behavior of the OFET) (Figure 1.5 a).

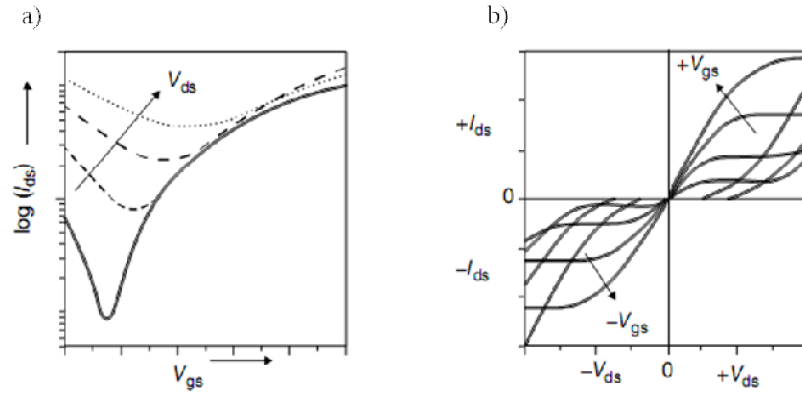


Figure 1.5 (a) Calculated transfer characteristics for an ambipolar transistor with equal hole and electron mobilities and slightly different threshold voltages in a semilog plot for positive gate voltages and different positive source-drain voltages. (b) Calculated ambipolar output characteristics for the same transistor for positive (first quadrant) and for negative (third quadrant) V_g and V_{ds} , respectively ^[4].

Since both charge carriers can flow through the channel, the I_{ds} output current does not completely saturate, but it is composed of two phases. In the first phase, when one charge carrier is flowing, the behavior is similar to that of a unipolar OFET, and eventually, the current can reach a temporary plateau. When the gate voltage reaches a local bias that permits the injection of the opposite charge carrier, the I_{ds} output current begins to raise quadratically (Figure 1.5 b). Within the graduate channel approximation, it is possible to derive a simple analytical expression for the ambipolar regime. If we assume an infinite recombination rate of holes and electrons, all injected holes and electrons have to combine and thus the source-drain current equals the electron and hole current for each channel. Combining the expressions for the saturated currents for the hole and electron channels, the source-drain current is given by:

$$|I_{ds}| = \frac{WC_i}{2L} \left\{ \mu_e (V_{gs} - V_c^e)^2 + \mu_h (V_{ds} - (V_{gs} - V_c^h))^2 \right\}$$

The position x_0 of the recombination zone within the channel is obtained by:

$$x_0 = \frac{L(V_{gs} - V_c^e)^2}{(V_{gs} - V_c^e)^2 + \frac{\mu_h}{\mu_e} (V_{ds} - (V_{gs} - V_c^h))^2}$$

The equation confirms that the position of the recombination zone, and therefore of the light-emitting area, depends on the applied voltages and on the ratio of the hole- and electron-mobility values.

1.5 Key building blocks of OFETs/OLETs

Dielectric layer

The crucial process of charge accumulation and transport in field-effect transistors takes place at and very close to the interface between the gate dielectric and the semiconductor, hence, the properties of this interface and of the dielectric material have a huge influence on device characteristics. Device parameter such as mobility, threshold voltage, etc. depend not only on the nature of the semiconductor but also on the chemical structure and properties of the insulator. Indeed the roughness and the polarity of the dielectric layer affect the morphology and the molecular arrangement of the semiconducting layer^{[26][27]}. Gate dielectrics are mainly characterized by their dielectric constant k , which determines the capacitance $C_i = \epsilon_0 k/d$ of a dielectric layer of thickness d (ϵ_0 is the permittivity in vacuum) and thus the amount of induced charges per applied gate voltage. Hence, in order to achieve a certain amount of charges in the transistor channel, one can either reduce the dielectric thickness or use a dielectric with a higher dielectric constants. High- k dielectrics are preferable for use in organic devices because they allow to scale down the device dimensions and lower the driving voltage^[28]. In addition gate dielectrics need to have low gate leakage current and the ability to sustain high voltage without dielectric breakdown.

The most common gate dielectrics used are Si substrates having SiO_2 layers (typically 200-400 nm-thick). The utilization of this dielectric is very convenient due to the ready availability of the thermally grown dioxide. Although, the presence of hydroxyl groups, which are present in the form of silanols, on the surface induce a large density of electron-trapping site. Surface treatments with hexamethyldisilazane (HMDS) or alkanetrichlorosilanes able to create a self-assembled monolayer (SAM) on the surface are often used in order to reduce these traps. In order to improve the electrical performance of organic electronic device, alternative metal oxides showing higher k with respect to SiO_2 ($k \approx 4$) have been employed, such as Al_2O_3 ($k \approx 8$), TiO_2 ($k \approx 41$), ZrO_2 ($k \approx 25$) etc.^[28]. Among the possible candidates for gate dielectrics, polymer insulators are highly promising because they exhibit not only ideal flexibility for flexible electronics but also promote intimate contact with the organic semiconductors^[5]. In this thesis both polymeric dielectric, such as polymethylmetacrylate (PMMA) and Cytop

(Figure 1.6), and inorganic high-k oxides were implemented as gate dielectric in OFET and OLET structures. Comprehensive reviews about dielectric materials for organic field-effect transistors are ^{[29][30][31]}.

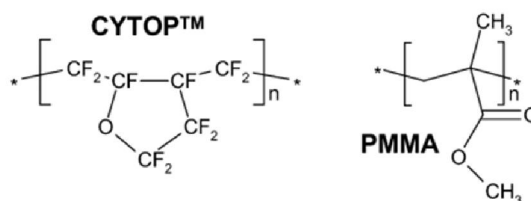


Figure 1.6 Organic polymers used as gate-dielectric in this work.

Active material

According to the molecular weight organic semiconductors can be divided in small-molecule and polymers. Small-molecule based materials have traditionally exhibited higher mobility values than conjugated polymers thanks to defined structures, the higher control of the level of purity and the long-range order molecular organization in thin films. As we said previously, organic semiconductors should support both electron and hole conduction equally. However, to date the majority of them are p-type conducting holes better than electrons. This is principally connected with the mismatch between the LUMO level of the organic semiconductor materials and the working function of the commonly environmentally stable electrodes (such as gold) used in device realization. The main strategy to reduce this mismatch and thus allow the easily injection of electrons into the organic semiconductor, is to reduce the LUMO energies by the introduction of electron-withdrawing groups such as halogen, cyano, carbonyl, etc. into the semiconductor molecular structures. Moreover, electron-withdrawing groups can increase the electron affinity of the materials as well as the air stability ^[5].

In addition to energetic considerations, the orientation of molecules to each other and the associated transfer integrals of electrons affect the device performance. In particular organic semiconductors can adopt four different kind of packing motif as shown in Figure 1.7: 1) herringbone packing (face-to-edge) without π - π overlap (face-to-face) between adjacent molecules (Figure 1.7 a), 2) herringbone packing with π - π overlap between adjacent molecules (Figure 1.7 b), 3) lamellar packing, one-dimension (1-D) π - π stacking (Figure 1.7 c), 4) lamellar packing, two-dimension (2D) π - π stacking (Figure 1.7

d). The most efficient packing for charge transport is the lamellar 2D π -stacking, since it can transport the charge carriers through an almost straight line ^[5].

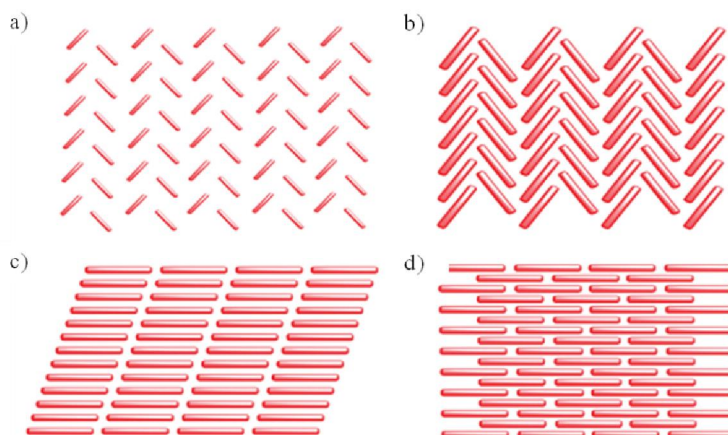


Figure 1.7 Molecular packing motifs in organic crystals ^[5].

Moreover, the molecules should be preferentially oriented with the long axes approximately parallel to the normal direction to the FET substrate since the most efficient charge transport occurs along the direction of intermolecular π -stacking and the crystalline domains of the semiconductor must cover the area between the source and drain contacts uniformly ^[1].

Excellent reviews report a complete discussion of OFET materials ^{[5][32][33]}.

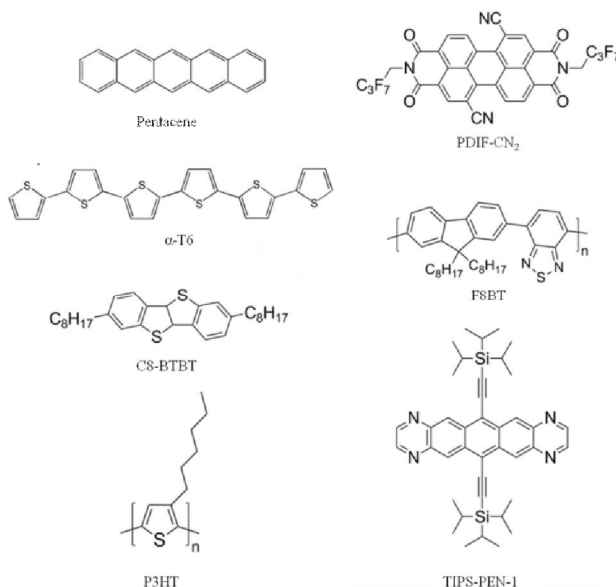


Figure 1.8 Organic π -conjugated semiconductors commonly used as active material in OFETs and OLETs.

Very briefly, the most commonly p-type semiconductors used in OFETs are based on linear acenes or oligoacenes and thiophene based polymers and oligomers. Many n-channel semiconductors are based on oligothiophenes, in which the molecular energy levels have been tuned by substitution with cyano, perfluoroalkyl/aryl, and alkyl/arylcarbonyl, naphthalene and perylene derivatives, phthalocyanine and fullerenes. Apart from few very efficient polymeric compounds as the spin-coated poly(9,9-dioctylfluorenealt-benzothiadiazole) (F8BT), main ambipolar semiconductors are obtained by small-molecules such as silylethynylated N-heteropentacenes TIPS-PEN^[34] or the natural pigment Tyrian Purple (6,6 ϕ -dibromoindigo)^[35] (Figure 1.8).

OLETs require the active materials to possess both high carrier mobility and high photoluminescence quantum yields (PLQYs). However, these two properties often exclude each other. In most cases, organic semiconductor systems that display high charge mobility due to the strong interchain/intermolecule interactions suffer from quenching luminescence in the solid state^{[21][36]}. This is the reason why only few materials allowing the fabrication of single layer are present in literature. To date, the polymeric ambipolar single-layer OLET based on F8BT reported by Gwinner et al^[37] represents the state-of-the-art for OLETs showing balanced electron and hole mobilities and emitting capability which achieved external quantum efficiencies >8%.

Injecting Electrodes

Before a current can flow through the transistor channel, charges have to be injected from the electrodes into the semiconductor: that means, for n-channel transistors, injection of electrons into the LUMO level and, for p-channel transistors, injection of holes into the HOMO level of the semiconductor. The metal-semiconductor interface is usually treated as a Mott-Schottky barrier, where the energy barrier is given by the difference between the metal work function and the semiconductors HOMO or LUMO level^[4] (Figure 1.9 a).

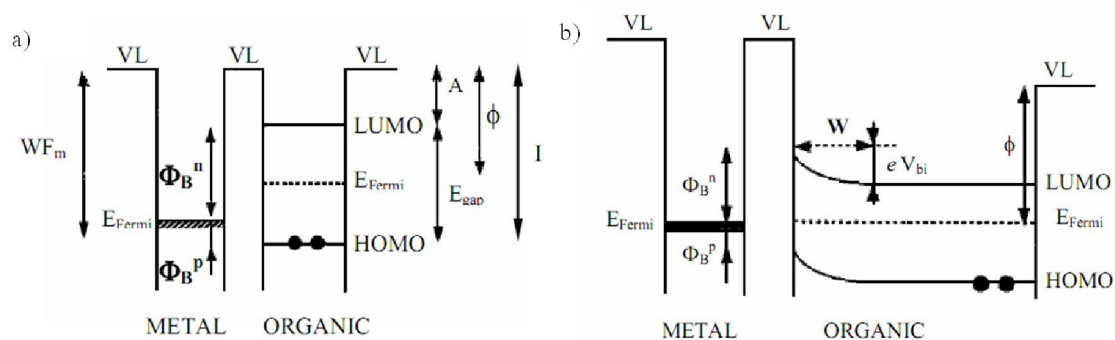


Figure 1.9 (a) Schematic representation of an ideal organic semiconductor/metal interface with WF_m metal working function, A organic semiconductor electron affinity, I ionization energy, E_{gap} energy band gap. Φ_B^p and Φ_B^n are the energy injection barrier for holes and electrons respectively and ϕ the work function of the organic material. (b) Energy level band bending at the organic semiconductor/metal interface. A diffusion layer of thickness W compares.

The barrier is formed after the contact between the metal and the semiconductor, and physically consists of a region of uncompensated charge. As a result, a diffusion layer compares and there is a bending of the energetic levels of the semiconducting material at the interface. When the work function of the injecting metal is close to the HOMO or LUMO level of the semiconductor, a good ohmic contact is achieved. Otherwise, a potential barrier is formed, leading to poor charge injection and non-ohmic contacts ^[38]. This is the reason why high work function metals (e.g. Au) are used for p-type conductor while low work function metals (e.g. Ca) are commonly preferred for n-type channel OFET. Although the simple Mott-Schottky model provides a guideline for choosing appropriate injecting electrodes, it is not sufficient to describe properly the charge injection into organic semiconductors and other models such as thermally-assisted tunneling from the metal into the localized states of the semiconductor were proposed ^[39]. Electrode materials can be manufactured from a variety of materials including metals (e.g. Au,Ag), heavily doped silicon, metallic conductive oxides (e.g. Indium Tin Oxide (ITO)), conductive polymers such as poly(3,4ethylenedioxythiophene) doped with poly(styrene sulfonate) (PEDOT:PSS) and grapheme ^[5].

References

- [1] A. Facchetti, *Mater. Res.* **2007**, *10*, 28.
- [2] J. Mei, Y. Diao, A. L. Appleton, L. Fang, Z. Bao, *J. Am. Chem. Soc.* **2013**, *135*, 6724.
- [3] H. Sirringhaus, *Adv. Mater.* **2014**, *26*, 1319.
- [4] J. Zaumseil, H. Sirringhaus, *Chem. Rev.* **2007**, *107*, 1296.
- [5] C. Wang, H. Dong, W. Hu, Y. Liu, D. Zhu, *Chem. Rev.* **2012**, 2208.
- [6] A. Tsumura, H. Koezuka, T. Ando, *Appl. Phys. Lett.* **1986**, *49*, 1210.
- [7] S. R. Forrest, *Nature* **2004**, *428*, 911.
- [8] G. Gelinck, P. Heremans, K. Nomoto, T. D. Anthopoulos, *Adv. Mater.* **2010**, *22*, 3778.
- [9] L. Torsi, M. Magliulo, K. Manoli, G. Palazzo, *Chem. Soc. Rev.* **2013**, *42*, 8612.
- [10] Z. Bao, J. Locklin, *Organic Field-Effect Transistors*, CRC Press, **2007**.
- [11] C. R. Newman, C. D. Frisbie, A. Demetrio, S. Filho, J. Bre, *Chem. Mater* **2004**, *16*, 4436.
- [12] L.-L. Chua, J. Zaumseil, J.-F. Chang, E. C.-W. Ou, P. K.-H. Ho, H. Sirringhaus, R. H. Friend, *Nature* **2005**, *434*, 194.
- [13] M. Muccini, S. Toffanin, *Organic Light-Emitting Transistors: Towards the Next Generation Display Technology*, Ed. Wiley-Science, Wise Co-Publication, **2016**.
- [14] J. Zaumseil, R. H. Friend, H. Sirringhaus, *Nat. Mater.* **2006**, *5*, 69.
- [15] M. Muccini, W. Koopman, S. Toffanin, *Laser Photonics Rev.* **2012**, *6*, 258.
- [16] S. Toffanin, R. Capelli, W. Koopman, G. Generali, S. Cavallini, A. Stefani, D. Saguatti, G. Ruani, M. Muccini, *Laser Photonics Rev.* **2013**, *7*, 1011.
- [17] A. Hepp, H. Heil, W. Weise, M. Ahles, R. Schmechel, H. von Seggern, *Phys. Rev. Lett.* **2003**, *91*, 157406.
- [18] C. Santato, R. Capelli, M. A. Loi, M. Murgia, F. Cicoira, V. A. L. Roy, P. Stallinga, R. Zamboni, C. Rost, S. F. Karg, M. Muccini, *Synth. Met.* **2004**, *146*, 329.
- [19] F. Dinelli, R. Capelli, M. A. Loi, M. Murgia, M. Muccini, A. Facchetti, T. J. Marks, *Adv. Mater.* **2006**, *18*, 1416.
- [20] R. Capelli, S. Toffanin, G. Generali, H. Usta, A. Facchetti, M. Muccini, *Nat. Mater.* **2010**, *9*, 496.

- [21] I. F. Perepichka, D. F. Perepichka, H. Meng, F. Wudl, *Adv. Mater.* **2005**, *17*, 2281.
- [22] K. Saxena, V. K. Jain, D. S. Mehta, *Opt. Mater. (Amst)*. **2009**, *32*, 221.
- [23] E. B. Namdas, B. B. Y. Hsu, J. D. Yuen, I. D. W. Samuel, A. J. Heeger, *Adv. Mater.* **2011**, *23*, 2353.
- [24] H.-H. Hsieh, W.-C. Chen, G. Generali, C. Soldano, R. DøAlpaos, G. Turatti, V. Biondo, M. Muccini, E. Huitema, A. F, in *Soc. Inf. Disp.*, **2016**.
- [25] M. Mas-Torrent, C. Rovira, *Chem. Rev.* **2011**, *111*, 4833.
- [26] F. Todescato, R. Capelli, F. Dinelli, M. Murgia, N. Camaioni, M. Yang, R. Bozio, M. Muccini, *J. Phys. Chem. B* **2008**, *112*, 10130.
- [27] W. H. Lee, J. H. Cho, K. Cho, *J. Mater. Chem.* **2010**, *20*, 2549.
- [28] P. Ortiz, A. Facchetti, T. J. Marks, R. P. Ortiz, A. Facchetti, T. J. Marks, *Chem. Rev.* **2010**, *110*, 205.
- [29] M. H. Yoon, C. Kim, A. Facchetti, T. J. Marks, *J. Am. Chem. Soc.* **2006**, *128*, 12851.
- [30] J. Veres, S. Ogier, G. Lloyd, *Chem. Mater.* **2004**, *16*, 4543.
- [31] A. Facchetti, M.-H. Yoon, T. J. Marks, *Adv. Mater.* **2005**, *17*, 1705.
- [32] H. Usta, A. Facchetti, in *Large Area Flex. Electron.*, Wiley-VCH Verlag GmbH & Co. KGaA, **2015**, pp. 16100.
- [33] S. Z. Bisri, C. Piliago, J. Gao, M. A. Loi, *Adv. Mater.* **2014**, *26*, 1176.
- [34] Z. Liang, Q. Tang, R. Mao, D. Liu, J. Xu, Q. Miao, *Adv. Mater.* **2011**, *23*, 5514.
- [35] M. Irimia-Vladu, E. D. G??owacki, P. A. Troshin, G. Schwabegger, L. Leonat, D. K. Susarova, O. Krystal, M. Ullah, Y. Kanbur, M. A. Bodea, V. F. Razumov, H. Sitter, S. Bauer, N. S. Sariciftci, *Adv. Mater.* **2012**, *24*, 375.
- [36] A. Dadvand, A. G. Moiseev, K. Sawabe, W. H. Sun, B. Djukic, I. Chung, T. Takenobu, F. Rosei, D. F. Perepichka, *Angew. Chemie - Int. Ed.* **2012**, *51*, 3837.
- [37] M. C. Gwinner, D. Kabra, M. Roberts, T. J. K. Brenner, B. H. Wallikewitz, C. R. McNeill, R. H. Friend, H. Sirringhaus, *Adv. Mater.* **2012**, *24*, 2728.
- [38] L. Bürgi, T. J. Richards, R. H. Friend, H. Sirringhaus, *J. Appl. Phys.* **2003**, *94*, 6129.
- [39] M. A. Abkowitz, H. A. Mizes, *Appl. Phys. Lett.* **1995**, *66*, 1288.

Chapter 2

Experimental setup

2.1 Thin-film deposition

Film growth methods can be generally divided into two groups: vapor-phase deposition and liquid-based growth^[1]. Thermal sublimation in high vacuum, is the typical method of thin-film preparation for small-molecule organic semiconductors because they often exhibit only low solubility, while growth from solution (e.g. spin-coating, inkjet printing and spray coating) are preferentially used for polymeric systems^[2]. The growth of organic molecule films is a non-equilibrium phenomenon, thus equilibrium or near equilibrium energy consideration alone cannot properly account for all growth scenarios and a dynamic description is needed. This description has to take in account the flux of molecules towards the surface, the adsorption and re-desorption probabilities and the diffusion process on the surface (interlayer and intralayer) and their respective barriers^[3] (Figure 2.1).

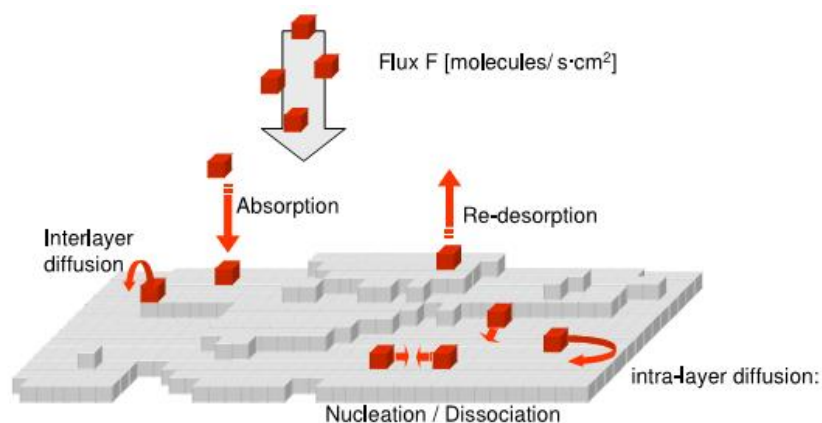


Figure 2.1 Schematic of atomistic processes relevant for Organic Molecular Beam Deposition^[2].

The interaction between film and substrate plays a very important role in determining the initial nucleation and the film growth ^[1]. There are three basic growth modes: island (Volmer-Weber), layer-plus-island (Stranski-Krastanov) and layer-by-layer growth (Frank-van der Merwe) as depicted in Figure 2.2. These growth modes depends to the surface energies $\gamma_{\text{substrate}}$, γ_{film} and $\gamma_{\text{interface}}$ ^[2].

Layer-by-layer mode of growth is the preferential mode for organic transistor realization because it leads to large, well connected domains that facilitate charge transport parallel to the substrate. It is thermodynamically favorable for systems where the sum of the surface energy of the adsorbate and the interfacial energy between the substrate and the film is less than or equal to the surface energy of the substrate. First complete monolayer is formed, before the deposition of second layer occurs. As the film grows thicker, the effective value of the substrate-film interfacial energy may increase enough to make layer-by-layer growth unfavorable and, eventually, lead to the Stranski/Krastanov growth mode whereby islands form on top of one or several complete monolayers. The growth scenario of Volmer/Weber occurs when the interfacial energy and the film surface energy are higher than the substrate surface energy.

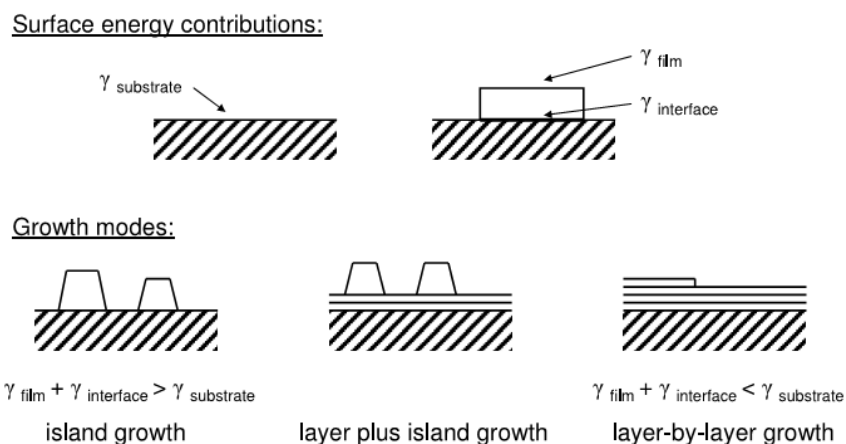


Figure 2.2 Growth modes of organic thin-films grown by thermal sublimation. Scenarios for thin film growth: depending on the material specific surface free energies three different generic growth modes are generally distinguished: island growth, layer plus island growth, and layer-by-layer growth ^[3].

There are some other considerations concerning the organic growth exclusively:

- As extended objects, organic molecules have internal degrees of freedom. Vibrational, conformational and orientational degree of freedom can give rise to an additional source of disorder with respect to the growth of atomic system.

New phenomena, such as the change of the molecular orientation during film growth may even lead to -lying down and -standing up structures.

- The interaction between molecules and between molecules and the substrate is often dominated by weak van-der-Waals forces. Thus, the response to strain is generally different: the weaker interactions per atom lead to -softer materials and, for example, strain can be accommodated more easily. The importance of van-der-Waals interactions implies that the relevant temperature scales (for evaporation from a crucible and also for diffusion on the substrate) are usually lower.
- The size of the molecules and the associated unit cells are greater than that of typical (inorganic) substrates. Moreover the organics frequently crystallize in low-symmetry structures, which can lead to multiple domains, which further increases the disorder.

Thermal sublimation

Vacuum sublimation has experienced an enormous diffusion in the last decades as a technique to prepare thin films of small molecule organic semiconductors^[4].

The main advantages of this technique consist of providing sub-monolayer thickness control during the growth, while the ultraclean environment provided by vacuum ensures a low level of contamination due to moisture or chemical impurities. Moreover, the presence of many control parameters give the possibility to drive a preferential growth modality. The main drawbacks of this technique are: high instrumental costs (turbomolecular pump, high vacuum chambers, etc.), impossibility to process polymers and high molecular weight materials, low industrial applicability and operational complexity.

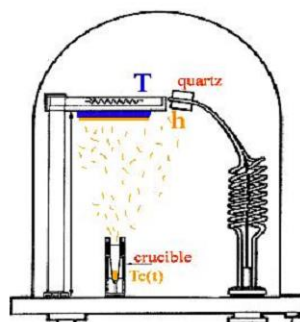


Figure 2.3 Scheme of a vacuum chamber for thermal sublimation of organic materials.

The core of every vacuum sublimation setup consists of a vacuum chamber with a crucible and a substrate held perpendicularly to the crucible orifice (Figure 2.3). The material is held in the crucible and heated to sublimation temperature. Once the crucible is filled with the material, it is heated until it is reached the sublimation temperature of the material. The material exits the crucible orifice as a molecular beam and impinges onto the substrate. Then, according to the substrate temperature, molecules can be adsorbed, desorbed or diffuse to a nucleation center. A quartz microbalance placed near the substrate is used to monitor the amount of material sublimed. Thus, the evaporation rate and the film nominal thickness can be easily calculated after an accurate calibration procedure. Evaporation rate and substrate temperature are a key parameters to modulate films morphology^[5].

The evaporation system used for film deposition presented in this thesis is the vacuum chamber depicted in Figure 2.4. It is a home-made chamber equipped with four Knudsen cells for evaporation and is connected to a glove-box. This configuration permits the sequential growth of the active material and of the top metal-contacts with immediate electrical characterization of the devices without any air exposure. The setup has a base pressure of 10^{-6} mbar thanks to a turbomolecular pump.

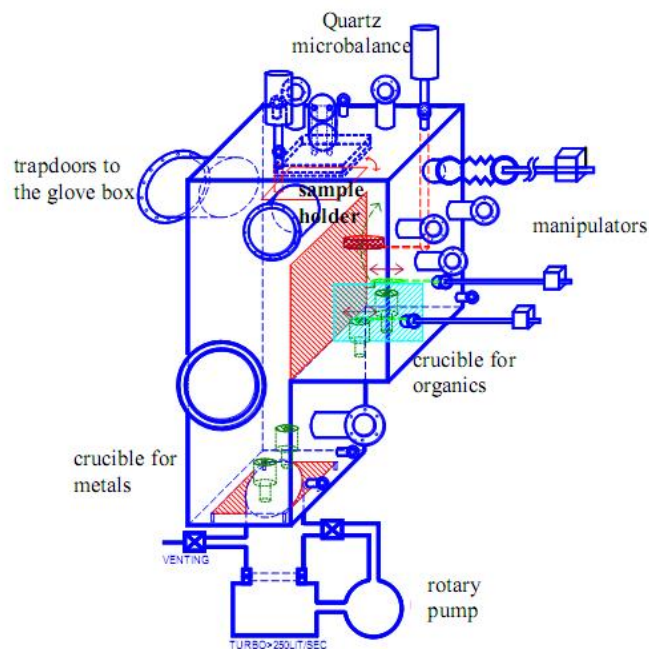


Figure 2.4 Scheme of the home-made vacuum chamber used in this work.

Supersonic Molecular Beam Deposition

In a Supersonic Molecular Beam Deposition (SuMBD) system, molecules to be deposited are seeded in a supersonic carrier gas molecular beam that, in specific conditions, is able to strongly accelerate them^[6]. The setup of a SuMBE source is sketched in Figure 2.5.

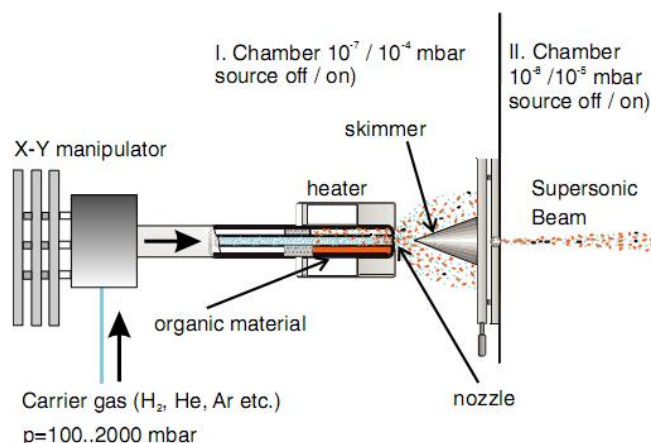


Figure 2.5 Setup of SuMBD source^[7].

The method allows for the preparation of well-collimated, highly directional beams of organic molecules with controlled kinetic energy from a fraction of eV to several tens of eV, while the kinetic energy of the beam and the thermal energy of the molecules are decoupled. It should be noted that due to the fast and efficient cooling caused by expansion the molecules (down to a few K) the roto-vibrational degrees of freedom are confined producing a molecular beam with a preferential alignment of the molecular backbone along the beam^[7]. SuMBD provide remarkable advantages with respect to a standard thermal sublimation. In particular, not only the intensity of the supersonic beam was far higher than conventional effusive beam, but the spreads in velocity and rotational states of the source molecules is markedly narrowed. Nowadays, molecular beams are used also for epitaxial growth of a wide variety of materials ranging from metal to oxide and organic or inorganic semiconductors.

Spin-coating

Spin-coating is a procedure used to apply uniform thin films to flat substrates. A small quantity of the solution is dispensed on the substrate, which is then rotated at high speed.

The spinning causes most of the solution to be ejected from the substrate immediately. As the solution dries, viscosity increases until the radial force of the spin process can no longer appreciably move the solution over the surface (Figure 2.6).

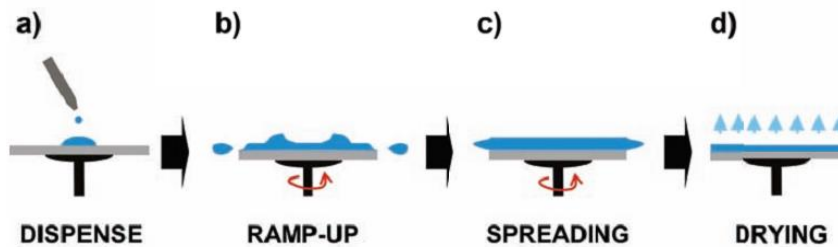


Figure 2.6 Spin-coating process

The spinner is stopped and generally the process is completed by evaporating the residual solvent in an oven ^[8]. By implementing this process it is possible to obtain a highly uniform μm on top of a planar substrate over a large area, with highly controllable and reproducible μm thickness. Physics behind the spin coating technique involve a balance between controlled centrifugal forces and viscous forces that are determined by solution viscosity. The main process parameters are: solution viscosity, angular speed (), angular acceleration, spin time and solution volume. Solution viscosity is determined by the concentration of the organic material and generally, very dilute solutions afford thin films while viscous solutions give rise to thick films. The spin speed of the substrate (rpm) affects the intensity of centrifugal force applied to the solution. Film thickness is largely a balance between the force applied to shear the solution towards the edge of the substrate and the drying rate. Film thickness does not decrease significantly when spin time increases. Generally, the higher the speed, the thinner the film. The acceleration of the substrate towards the final spin speed can also affect the coated film properties. Since the solution begins to dry during the first part of the spin cycle, it is important to accurately control acceleration. Spin-coating represents a useful technique to process in particular polymers, which are not compatible with sublimation process and whose solubility is high in many solvents.

Lithographically Control Wetting

Lithographically Control Wetting (LCW) is a simple and fast wet-patterning process based on a stamp-assisted deposition. LCW exploits the self-organization of soluble

materials, permitting spatial control provided by the features of a stamp (Figure 2.7). This technique is suitable for large-area nanopatterning, and is sustainable because of its simplicity, high transfer rate, and low cost of materials and equipment ^[9]. In fact, it yields nanometer-sized structures in a few seconds and in a single step.

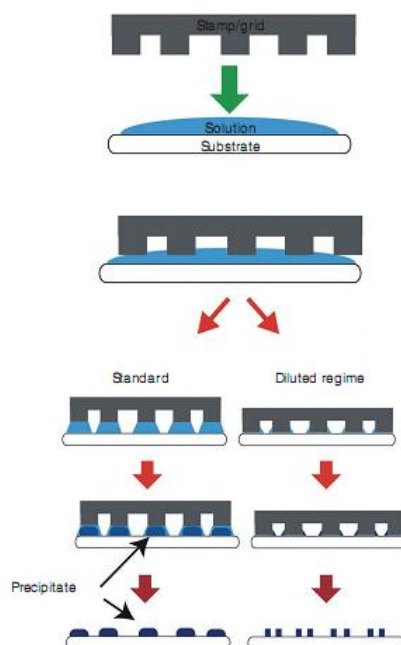


Figure 2.7 Scheme of Lithographically Controlled Wetting (LCW). Scheme of printing using a floating stamp in the standard (right) or diluted (left) regime. Whereas in standard conditions features with size comparable to the stamp protrusions are printed, in the diluted regime a split of the printed features with reduced size takes place ^[10].

The stamp can be made of either rigid materials, such as metals, ceramics or rigid polymers, or by soft materials, such as polycarbonates or PDMS. Moreover, using suitable stamps, this technique can be used also with aggressive chlorinated and fluorinated solvents. When a stamp is placed in contact with a liquid thin film spread on a substrate, an instability of the fluid layer develops, where capillary forces pin the solution to the stamp protrusions, giving rise to an array of menisci. As the solvent evaporates and the critical concentration is reached, the solute precipitates onto the substrate within the menisci, giving rise to a structured thin-film that replicates the protrusion of the stamp ^[10]. The choice of concentration of the solution is crucial for the effectiveness of the result. In particular low concentration regimes, the menisci can be splitted under the same protrusion thus obtaining smaller structures.

2.2. Device fabrication

Single-layer top contact/bottom gate transistors were fabricated on glass/ITO substrate where ITO works as a gate electrode. ITO substrates were cleaned by ultrasonic baths in acetone and 2-propanol before deposition. The 450 nm thick dielectric layers of PMMA or Cytop have been deposited by spin-coating on top of the clean ITO substrates. The PMMA and Cytop films were then thermally annealed in a vacuum oven at 120°C for 15 hours and 1 hour, respectively ($C_{\text{PMMA}} = 7.08 \text{ nFcm}^{-2}$, $C_{\text{Cytop}} = 3.99 \text{ nFcm}^{-2}$). The organic active layer of NT4N have been grown by vacuum sublimation in a home-made vacuum chamber, with a deposition rate of 0.6 nm/min at a base pressure of 10^{-6} mbar. The substrate temperature during the film deposition has been kept at room temperature (RT). The drain-source electrodes were made of gold and were evaporated through a shadow mask on top of the organic thin films. The gold layer thickness is 70 nm, while the channel length and the channel width are 70 μm and 15 mm, respectively.

Single-layer top contact/bottom gate transistors comprising the multilayer photonic crystal as gate dielectric (ML-PhC) on glass/ITO substrate were realized following the same procedure. The photonic structure consists of PMMA-functionalized stack of alternating layers of ZrO_2 and Al_3O_2 . The ML-PhC has been fabricated by PLD deposition at the IIT of Milano. This technique is based on a pulsed excimer laser (KrF with $\lambda=248 \text{ nm}$ and repetition rate of 20 Hz) focused on a target of the employed materials that are vaporized. Further details of the technique are described in [11].

Bilayer top contact/bottom gate transistors were fabricated on glass/ITO substrates where ITO works as a gate electrode and PMMA (450nm) is used as a gate dielectric. The organic active region consists of a stacked bilayer formed by a high-mobility p-type semiconductor C8-BTBT (45nm at 0.6 nm/min) in direct contact with the dielectric layer and a compact thin-film made of anthracene derivative (60nm at 6 nm/min). The organic bilayer stack and the on-top metal electrodes were deposited by thermal sublimation by means of shadow masks in a home-made high-vacuum deposition chamber at room temperature at a base pressure of 10^{-6} mbar. 70 nm thick silver source and drain electrodes were then sublimated. Devices have the following characteristics: 12 mm channel width, 70 mm channel length.

Single-layer bottom contact/bottom gate transistors were fabricated on multilayered substrates composed of a 500 μm thick layer of highly doped Silicon (Si^{++}) acting both

as gate and substrate, a 200 nm thin SiO₂ dielectric barrier and, finally, interdigitated source/drain gold electrodes (about 130 nm high) (W/L ratio was fixed to 550 where W is the channel width while L is the channel length). Substrates were functionalized with Hexamethyldisilazane (HMDS). 30 nm thick NT4N layer was grown by thermal sublimation/supersonic molecular beam deposition.

Top contact/bottom-gate transistors were fabricated by Lithographically Controlled Wetting on glass/ITO substrates where ITO works as a gate electrode and Cytop (450 nm) is used as a gate dielectric. The polydimethylsiloxane (PDMS) stamps were fabricated with Sylgard 184 Dow Corning by replica molding of an aluminium master. The curing conditions were: temperature 50° C and curing time 12 hours. After curing, the stamps were washed with pure CHCl₃ (Aldrich 99.8%) in order to remove the uncured material. We used stamps with parallel lines 1 μm wide. Saturated solutions of C6-NT4N in anisole and 1,2 dichlorobenzene were prepared and filtered with syringe filters of polytetrafluoroethylene (0.45 μm) before use. Devices were prepared by drop-casting 5 μl of the solution on the substrate. Top metal electrodes were then deposited by thermal sublimation by means of shadow masks in a home-made high-vacuum deposition chamber at room temperature at a base pressure of 10⁻⁶ mbar. Devices have the following characteristics: 12 mm channel width, 20 μm channel length, and 500 mm wide source and drain electrodes. All the process was carried out into a glovebox.

2.3 Thin-film characterization

Since both the morphology and the molecular arrangements in organic semiconducting layer play significant roles in the performance of OFETs, before the device optoelectronic characterization, structural, morphological and optical characterization of the active materials in thin-film were performed. Here the measurement setups and conditions used in this work are reported.

UV-visible absorption spectra were recorded using a JASCOV-550 spectrophotometer. Steady-state photo-luminescence (PL) was excited using a CW He-Cd laser and collected under transmission conditions (no color filter was necessary for truncating laser excitation). PL emission was collected using a calibrated optical multichannel analyzer (PMA-11, Hamamatsu).

Quantum yield measurements of thin-films were carried out using a stand-alone and automatic absolute PL Quantum Yield (PLQY) measurement System (C9920-02, Hamamatsu). The measurements were performed under ambient conditions and by exciting the PL emission at the thin film absorption maximum wavelength.

X-ray data were collected using a PANalytical X'Pert PRO powder diffractometer with Cu K α ($\lambda = 1.5418 \text{ \AA}$) as the incident radiation and a fast X'Celerator detector.

Morphological AFM characterization was performed at room temperature in air ambient by means of an XE100 Park instrument, operating in non-contact mode (amplitude modulation, silicon nitride cantilever from Nanosensors)

2.4 Device optoelectronic characterization

The device optoelectronic characterization was carried out by an Agilent B1500A Semiconductor Device Analyzer, using a standard SUSS Probe Station equipped with a Hamamatsu photodiode for light detection. The measurements were performed in a MBraun nitrogen glovebox since air and moisture could be disastrous in terms of device performances due to interaction with the organic layers.

A glovebox is a sealed container designed to allow one to manipulate objects while being in a controlled atmosphere that is usually a very high purity inert atmosphere (such as argon or nitrogen). Inert atmosphere gloveboxes are typically kept at a higher pressure than the surrounding environment, so any microscopic leaks are mostly leaking inert gas out of the box instead of letting air in. Built into the sides of the glovebox are gloves, arranged in such a way that one can place his hands into them and be able to perform tasks inside the box without breaking the seal or allowing potential injury to the worker. Our glovebox is composed of two containers coupled together (Figure 2.8). On one side two access entry chambers are present. The opposite side is linked to a growth chamber. This permits electrical characterization immediately after the device growth, without any air and oxygen exposure. Our glove box ensures oxygen and water presence below 0.1 ppm.

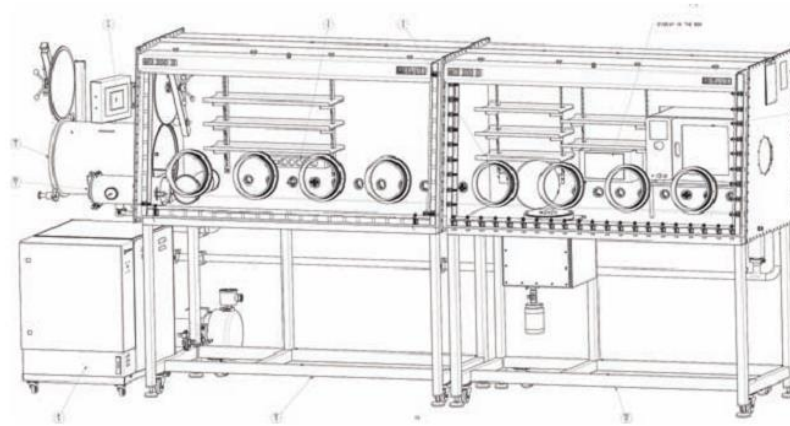


Figure 2.8 Scheme of the glovebox used in this work for device fabrication and characterization.

Inside the glovebox a probe station is located: by micrometric positioning of tungsten tips on the device pads we are able to apply voltage to device and collect even low-current signal (nA), with a noise level of pA. Electroluminescence measurements are possible since a photodiode is placed in the proximity of the device active area. An optical microscope is mounted vertically on the chuck plate to allow precise positioning of the probing tungsten tips on the device electrodes by using manual probeheads.

Optical characterization of the devices was also carried out in air. Before this characterization the as-fabricated devices were encapsulated inside the glovebox using a glass cover slip and an ultra violet cured epoxy sealant in order to prevent any deterioration of the sample.

The brightness measurements were performed by using a standard calibrated CS200 Konica Minolta spectroradiometer.

Angular emission profile was collected in a home-made setup. The sample was fixed at a Physik Instrument high-precision servomotor rotation stage which is controlled by a Labview program able to acquire the EL signal at any angle (range from -110° to 110°) by using a Hamamatsu pre-amplified photomultiplier tube (PMT). The angular resolution is about 5° . It is related to the distance between the emitter and the detector that has to be 10 times the highest dimension of the light source. This is important to consider the device a point-like light source so that the variations in the angular profile are not due to device geometry but only to different exciton distributions.

References

- [1] G. Cao, *Nanostructures and Nanomaterials. Synthesis, Properties, and Applications*, Imperial College Press, **2004**.
- [2] S. Kowarik, A. Gerlach, F. Schreiber, *J. Phys. Condens. Matter* **2008**, *20*, 184005.
- [3] F. Schreiber, *Phys. Status Solidi* **2004**, *201*, 1037.
- [4] S. R. Forrest, *Nature* **2004**, *428*, 911.
- [5] G. Generali, F. Dinelli, R. Capelli, S. Toffanin, F. Di Maria, M. Gazzano, G. Barbarella, M. Muccini, *J. Phys. Chem. C* **2011**, *115*, 23164.
- [6] F. Chiarella, T. Toccoli, M. Barra, L. Aversa, F. Ciccullo, R. Tatti, R. Verucchi, S. Iannotta, A. Cassinese, F. Chiarella, T. Toccoli, M. Barra, L. Aversa, F. Ciccullo, R. Tatti, R. Verucchi, *Appl. Phys. Lett.* **2014**, *104*.
- [7] K. Walzer, T. Fritz, K. Leo, *Surf. Sci.* **2006**, *600*, 2064.
- [8] C. J. Lawrence, *Phys. Fluids* **1988**, *31*, 2786.
- [9] Massimiliano Cavallini, C. Albonetti, F. Biscarini, *Adv. Mater.* **2009**, *21*, 1043.
- [10] M. Cavallini, D. Gentili, P. Greco, F. Valle, F. Biscarini, *Nat. Protoc.* **2012**, *7*, 1668.
- [11] D. Natali, J. Chen, F. Maddalena, F. Garcia Ferrer, F. Di Fonzo, M. Caironi, *Adv. Electron. Mater.* **2016**, *2*, 1.

Chapter 3

Correlation between crystalline phase and field-effect charge transport in ambipolar small-molecule thin-films

3.1 Introduction

The use of linear conjugated oligomers as active materials in field-effect organic transistor guarantees, in principle, higher electrical performances with respect to polymers thanks to the long-range order molecular organization achievable in thermally sublimated thin films ^[1]. Moreover, small molecules present the advantages of defined structures, higher control of the level of purity by exploiting conventional purification techniques, and batch to batch reproducibility. A promising conjugated molecular semiconductor, 2,2'-(2,2'-bithiophene-5,5'-diyl)bis(5-butyl-5H-thieno[3,2-c]pyrrole-4,6-dione), namely NT4N (Figure 3.1 a) was recently synthesized by the group of Manuela Melucci at the CNR-ISOF in Bologna ^[2]. NT4N belongs to the emerging class of thieno(bis)imide end substituted oligothiophenes (TBIs) which combines ambipolar charge transport capability to simultaneous electroluminescence. The group of research where I spent my PhD internship investigated the optoelectronic properties of NT4N in thin-film field-effect transistor demonstrating that the insertion of 2,3-thienoimide moieties as end groups in thiophene oligomers constitutes a viable design strategy to switch p-type unipolar and non-electroluminescent thiophene-based materials, to ambipolar and electroluminescent ones ^{[3][4]}. In particular, 2,3-thienoimide symmetric end-substitution strongly affects the LUMO distribution and energy levels with respect

to conventional oligothiophenes and promotes π - π stacking packing motif rather than the herringbone one, which is commonly related to enhanced charge transport capability in molecular semiconductors.

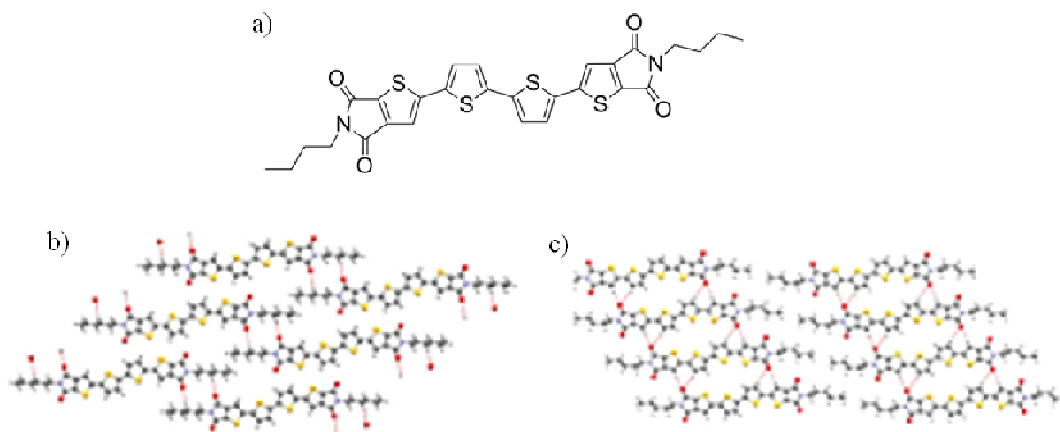


Figure 3.1 (a) Chemical structure of NT4N material. A view normal to the main molecular plane: NT4N phase A (b) and phase B (c) ^[5].

Moreover, NT4N derivatives having even chain ends presents two possible molecular conformation (anti-anti-anti and syn-anti-syn) according to the conformational arrangement of the two inner thiophene rings and the thienoimide substituents. The two conformational polymorphs adopt different molecular packing, namely phase A and phase B ^[5] (Figure 3.1 b and c). Giving these structural characteristics, NT4N is used as active layer in the fabrication of ambipolar single-layer Organic Light-Emitting Transistors (OLETs) and Organic Field-Effect Transistors (OFETs). Devices realized by thermal sublimation in high vacuum adopt selectively phase B. It was demonstrated the possibility to obtain phase A by drop-casting deposition from toluene ^[5] but up to now, no charge conduction has been demonstrated for this phase.

The first objective of this work was to validate the fabrication and characterization protocol of NT4N-based OLETs realized by thermal sublimation in high vacuum in order to enable the device platform for further implementation into optoelectronic applications. Then I investigated the strict correlation between the structural arrangements in solid state and the optoelectronic performance in NT4N-based thin-films realized by different deposition techniques.

3.2 NT4N as active material in ambipolar single-layer OLETs

A top contact/bottom gate (TC/BG) OLET structure comprising 30 nm of NT4N as active material was implemented as reference (Figure 3.2 a). A 450 nm thick polymethylmetacrylate (PMMA) film that works as dielectric layer is spin-coated on top of a transparent substrate functionalized with Indium Tin Oxide (ITO) that works as gate electrode. The active layer is deposited on top of the dielectric layer by means of thermal sublimation in high vacuum chamber (10^{-6} mbar) at a deposition rate of 0.6 nm/min. Finally, 70 nm-thick gold electrodes were sublimated on top of the semiconductor with a source-drain channel length of $L = 70$ nm and a channel width of $W = 1.2$ cm using a shadow mask process.

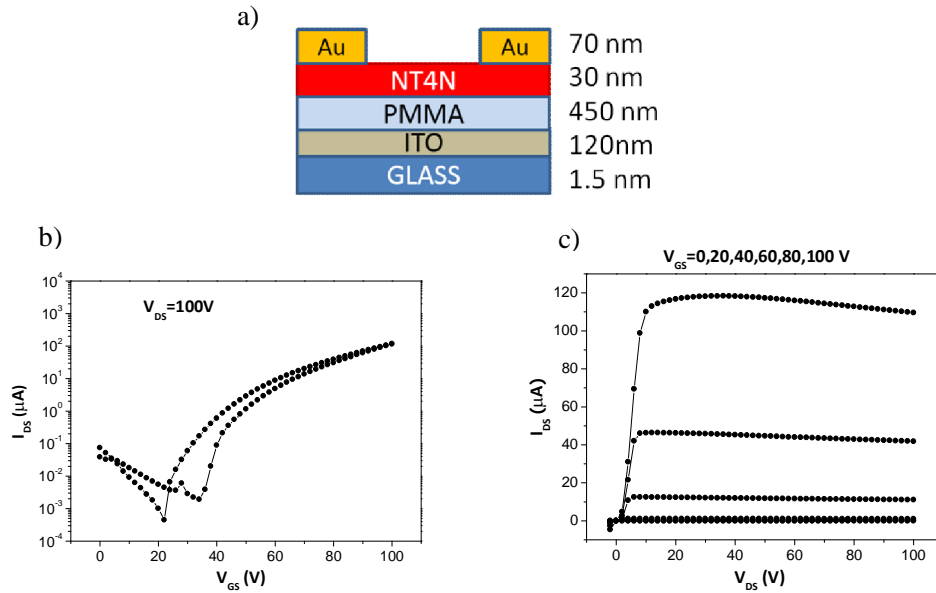


Figure 3.2 Schematic structure of a single-layer TC/BG NT4N based OLET (a). Electrical characterization performed on single-layer TC/BG OFET based on 30 nm of NT4N: (a) n-type transfer saturation curve, (b) n-type multiple output curves.

Standard electrical characterization for transistor devices was performed to investigate the charge transport properties of NT4N thin-film in field-effect transistor configuration (Figure 3.2 b e c). As expected, the device showed ambipolar behaviour with electron and hole mobility of $8.4 \cdot 10^{-2} \text{ cm}^2 \text{ V}^{-1} \text{ s}^{-1}$ and $2.5 \cdot 10^{-4} \text{ cm}^2 \text{ V}^{-1} \text{ s}^{-1}$, respectively. The device exhibits a $I_{on/off}$ ratio of 10^5 . Unfortunately, the thresholds voltage for both electrons and holes are high ($V_t^e = 49.1$ V, $V_t^h = -68.8$ V) and the p-type mobility is well-unbalanced with respect to n-type mobility.

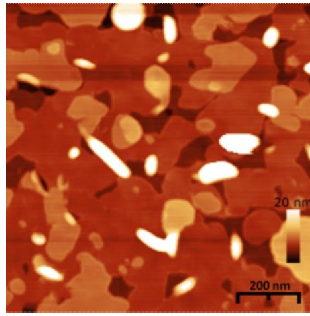


Figure 3.3 AFM image of 30nm-thick film of NT4N on PMMA.

The film morphology is shown in Figure 3.3. The AFM image highlights the coexistence of two different growth modes. Large islands start to form before the complete coverage of the underlying layers. Moreover tridimensional aggregates are observed.

In order to optimize the device performances, the active layer thickness were varied. The devices show a peculiar trend in the optoelectronic performance: by reducing the thickness of the active layer under 15 nm, the optoelectronic characteristics worsened, i.e. the mobility (both n-type and p-type) decreases by an order of magnitude. Surprisingly, the devices exhibit an improvement in the charge mobility and optical emitted power with the increase of thickness (Figure 3.4). Our group is currently investigating NT4N thin-film cristallinity and morphology at varying active layer thickness by means of Grazing-Incidence Small-Angle X-ray Scattering (GISAXS) and atomic force microscopy in order to better understand the trend observed in optoelectronic performances.

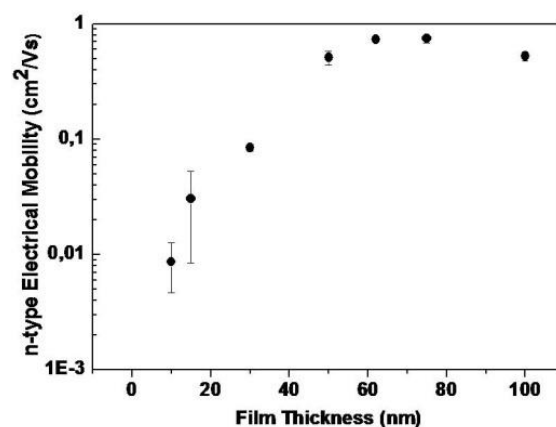


Figure 3.4 Electron mobility extracted from saturation transfer characteristic curves on TC/BG NT4N based devices with different thickness in the range 2-100 nm. All values are averaged using a large number of OLETs (over 100 devices) in order to improve the statistics.

The best performing device were obtained depositing 75 nm-thick NT4N layer: a maximum electron mobility of $1.09 \text{ cm}^2\text{V}^{-1}\text{s}^{-1}$ was measured. It is worth to note that the mobility value obtained is comparable with the state-of-the-art for unipolar single-layer OFETs based on n-type small molecule^[6]. 75nm-thick device presents a clear ambipolar behavior as evidenced by the V-shaped saturation transfer characteristic reported in Figure 3.5 a. The electroluminescence (EL) is maximized in the unipolar regime ($V_{DS} = V_{GS} = 100\text{V}$), indeed light emission is mainly located in the proximity of the charge-carrier injecting electrode. However, EL saturation transfer characteristics curve presents a shoulder in correspondence to the ambipolar region ($V_{GS} \sim 1/2V_{DS}$) where the balance between the hole and electron current is maximized and also the EL output characteristics curve (Figure 3.5 b) shows indication of ambipolar transport regime.

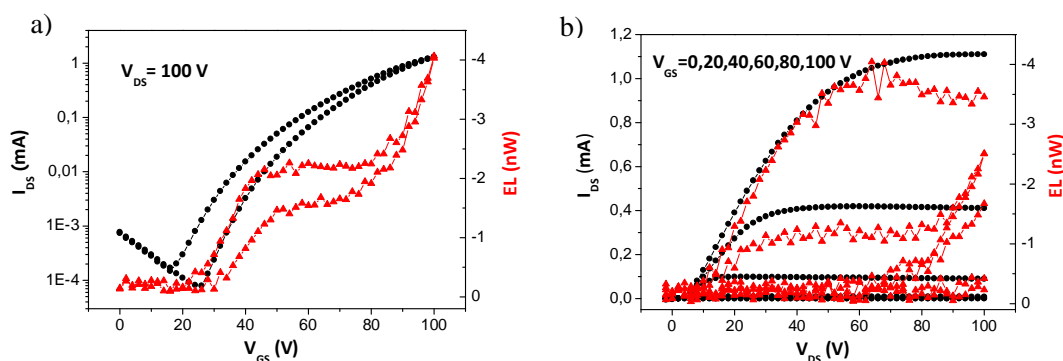


Figure 3.5 Electrical characterization performed on single-layer TC/BG OFET based on 75nm of NT4N: (a) n-type transfer saturation curve, (b) n-type multiple output curves.

As expected for an ambipolar material, the emission occurs within the channel in the proximity to the drain electrode, as a consequence of the difference between hole and electron mobility. However, the electroluminescence emission zone is well separated from the drain edge, preventing optical coupling of the emitted light with the metal electrodes.

3.3 Processing-structure-function correlation in NT4N-based thin-films

It is well-known that, owing to the weak interaction energies, small organic molecules are prone to polymorphism in the solid state^[7]. In recent years the study and control of polymorphism has gained growing interest in organic electronic applications^{[8][9][10]}. Optoelectronic properties are indeed intimately related to the structure and packing that

the materials adopt in the solid state and different structure of organic film can strongly influence device performance ^[11]. Several examples are reported in literature for pentacene, rubrene and oligothiophene semiconductors ^{[12][13][14]}. Among the others, also NT4N derivatives present two polymorphic forms. Given the characteristic above depicted, NT4N represents an ideal platform for an effective and exhaustive study of the correlation between charge transport properties and structural features in solid state.

In this study, we aim at investigating the deep packing-charge transport correlation in NT4N-based thin-films by implementing different deposition techniques such as thermal sublimation in high vacuum chamber, supersonic molecular beam deposition (SuMBD) and wet soft-lithography. Indeed, it is well-known that different crystal structures can be easily obtained by varying crystallization conditions, post-synthesis treatments or film deposition procedures ^{[15][16]}.

As dry deposition techniques, beside thermal sublimation which represents the standard protocol adopted for the realization of NT4N based OFETs (see previous paragraph), SuMBD was chosen. This technique gives the possibility to regulate the initial stage of the molecular precursors in the beam and in particular the kinetic energy, to control the morphology, structure and functional properties of the growing films ^[17]. In a SuMBD system, molecules to be deposited are seeded in a supersonic carrier gas molecular beam that, in specific conditions, is able to strongly accelerate them. This technique permits to reach kinetic energy of the molecules impinging the growth surface of several eV, much higher with respect to the typical values characterizing the depositing molecules in the classical sublimation technique. Several parameters such as the type and the pressure of the carrier gas, the molecular mass and dilution degree in the supersonic molecular beam influence the value of the achievable kinetic energy ^[18]. This technique was exploited in the realization of highly performing p-type ^[19] and n-type ^[18] organic thin-film transistor as well as to control the deposition of different polymorphic phases in titanylphthalocyanine layers ^[20]. Indeed, setting the kinetic energy of the organic material in the molecular beam is an effective strategy to activate specific film growth modes and to control the deposition of different polymorphs ^[15].

As wet technique, Lithographically Control Wetting (LCW) was adopted. LCW is a simple and fast wet-patterning process based on a stamp-assisted deposition ^[21]. When a stamp is placed in contact with a liquid thin film spread on a substrate, an instability of the fluid layer develops, in which capillary forces pin the solution to the stamp

protrusions, giving rise to an array of menisci. As the solvent evaporates and the critical concentration is reached, the solute precipitates onto the substrate within the menisci, giving rise to a structured thin-film that replicates the protrusion of the stamp. With respect to a conventional drop-casting, the shrinkage rate is slower and thus quasi-equilibrium conditions are achieved during solvent evaporation. The nature of the solvent, the capillary flow and evaporation rate, the solute intermolecular interactions and the interactions with the substrate determine the morphology and structure of the printed features ^[22]. Therefore the motif morphology can be substantially changed by changing only one parameter of the system. LCW has been successfully employed for the realization of OFETs since it enables the growth of the active material in a specific direction, i.e. between the electrodes. Moreover, this technique leads to oriented nanostripes with well-defined domains where physical properties of materials, such as charge transport, can be enhanced by controlling the organization ^[23].

For this study C4-NT4N and C6-NT4N derivatives were chosen. The increase of the alkyl substituent length does not affect the optical, self-assembly and charge transport properties of NT4N material ^[4], but it helps to increase the solubility of the compounds, thus enabling an effective deposition of the nanostructured films.

As a characterization protocol of the deposited thin-films, X-Ray Diffraction (XRD), Atomic Force Microscopy (AFM) and steady-state photoluminescence (PL) analysis were carried out on the fabricated samples and devices in order to investigate the structure and the morphology of the phase obtained. Then standard electrical characterization of the field-effect transistor devices was performed in nitrogen atmosphere to investigate the charge transport properties in controlled conditions.

SuMBD

Using supersonic molecular beam it was possible to increase the kinetic energy of the molecules impinging the growth surface leading to a variation of process dynamics with respect to the thermal sublimation technique. In particular, a value of kinetic energy $E_k = 12.4$ eV was used. Technical issues, and in particular the impossibility to realize a top contact configuration by SuMBD without breaking the vacuum, prevented a direct comparison with the TC/BG benchmark device described in the previous paragraph. A bottom contact/bottom gate (BC/BG) configuration on Si/SiO₂ usually used in SuMBD

[18][24] was chosen. Transistors were fabricated by the deposition of 30 nm of C4-NT4N on multilayered substrates composed of a 500 nm thick layer of highly doped Silicon (Si++) acting both as gate and substrate, a 200 nm thin SiO₂ dielectric barrier and, finally, interdigitated source/drain gold electrodes (about 130 nm high) (W/L ratio was fixed to 550 where W is the channel width while L is the channel length). Substrates were modified with Hexamethylsiloxane (HMDS) self-assembled monolayer obtained with a process lasting 7 days and described in detail in [25]. The functionalization is necessary to avoid electron trapping at the interface between the organic semiconductor and the dielectric [26]. Moreover, it guarantees a hydrophobic interface similar to the PMMA one suitable for NT4N growth. In order to compare the two dry techniques chosen, BC/BG NT4N based OLETs were realized by thermal sublimation as reference. Although the present study has demonstrated that the best optoelectronic performance for NT4N based device are obtained for a 75 nm-thick active layer (see paragraph 3.2), here a thickness of 30nm was chosen. Indeed, it represents a good trade-off between high mobility and acceptable time of deposition.

As expected from thermal sublimation, phase B was obtained (Figure 3.6 a). XRD analysis confirms that this process of deposition leads selectively to polymorph B, independently from the dielectric used.

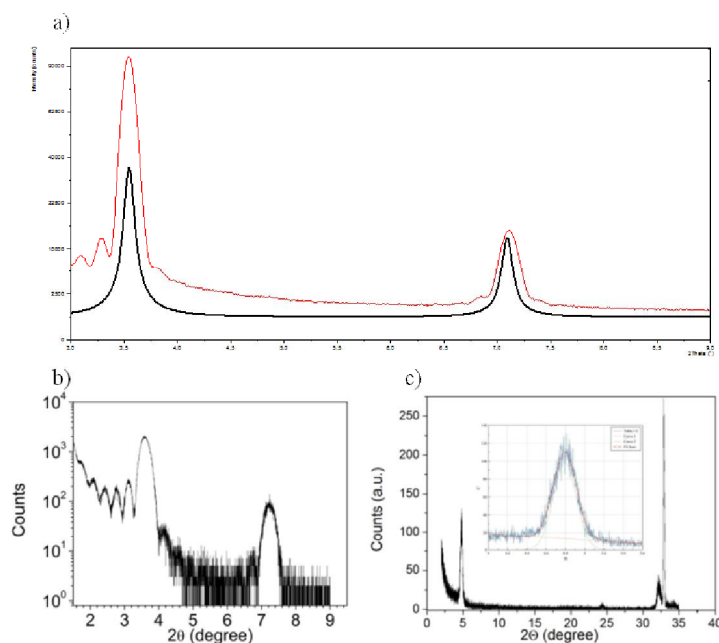


Figure 3.6 (a) X-ray spectra of C4-NT4N thin film on Si/SiO₂/HMDS by thermal sublimation (red line), theoretical X-ray spectra of C4-NT4N phase B (black line) is reported as comparison. X-ray spectra of C4-NT4N thin film on Si/SiO₂/HMDS by SuMBD at high (b) and low (c) deposition rate.

BC/BG devices were realized by SuMBD using 30nm of NT4N deposited at a rate comparable to the one adopted for thermal sublimation, 0.6 nm/min. As demonstrated in Figure 3.6 b, phase B was obtained. Interestingly, decreasing the deposition rate to 0.1 nm/min, SuMBD enables to obtain a new phase, namely phase X. The XRD pattern (Figure 3.6 c) presents a unique pick at low angles (about 4.8°) which is not compatible with the other known polymorphs. This packing was revealed here for the first time but, until now, it is not possible to obtain experimentally a single crystal presenting this structure and thus information about the molecular arrangement are not available.

Photoluminescence characterization of the thin-film was carried out (Figure 3.7). The spectrum of the sample deposited at high rate presents the characteristic PL emission features expected for phase B, with a maximum intensity emission at about 603 nm, red-shifted with respect to the spectrum of the molecule in solution. Interestingly, the sample deposited at low rate presents different emission profile with respect to the characteristic PL emission of known polymorphs^[5], with a blue-shift in the main emission peak of about 90 nm with respect to PL spectrum of the molecule in solution. PL measurements confirm the possibility to obtain two different phase by tuning the rate deposition, moreover the different shift shown in thin-film highlights a different molecular arrangement and intermolecular interactions in the two cases.

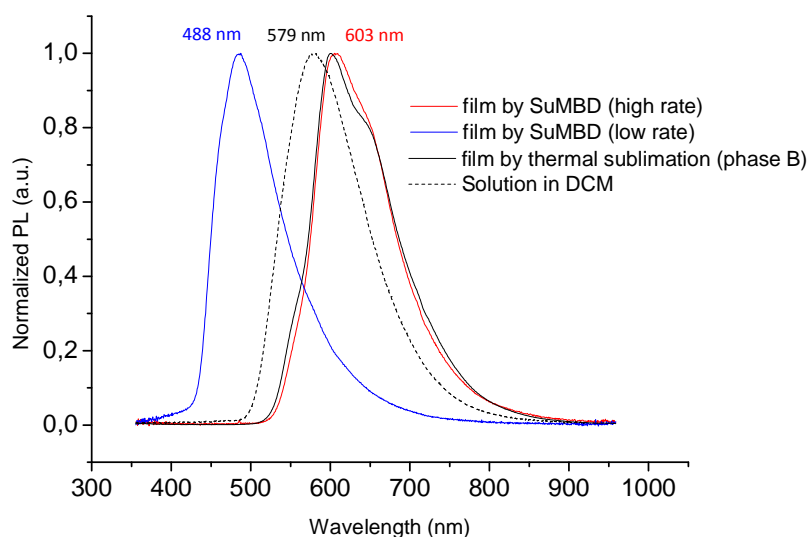


Figure 3.7 PL spectra of C4-NT4N thin-film deposited on quartz by thermal sublimation (black solid line), by SuMBD at high rate (red line) and low rate (blue line). PL spectrum of C4-NT4N in dichlorometane is reported as comparison (dashed line).

Indeed, when molecules are brought close together, like in solid state, the dipoles interact and multiple excitation energy levels are observed. The splitting of energy levels, Davydov splitting, is determinate by the difference between interacting transition dipole moments, their relative orientation and the number of interacting molecules ^[27]. In a simple model comprising only two molecules the excited energy state has two possible levels according to the phase relationship between the transition dipole moments. Depending on the relative orientation of the two molecules, and thus on the orientation of the monomer transition moments, only one transition can be allowed and the spectral shift can be either to the blue or to the red region of the spectrum with respect the monomer emission ^[28]. Indeed, this is exactly the scenario that we observed in the case of C4-NT4N deposited at different deposition rates by using SuMBD when we compare the spectral features of the photoluminescence of the films with C4-NT4N in solution (that can be considered as the monomer emission). Different supramolecular organizations in oligothiophenes have already been demonstrated by PL spectroscopy ^[29]. It is important to note that the two molecular packing motifs are achievable by tuning the deposition rate independently from the substrate: the same XRD pattern is observed both for Si/SiO₂/HMDS and quartz substrate used in the optical characterization. Thus, the new phase is achievable by the specific kinetic regime obtained by SuMBD.

AFM analysis were then carried out in order to investigate the morphology of all the thin-film realized. AFM analysis of NT4N deposited by SuMBD at low rate (Figure 3.8 a) shows rounded islands uniformly distributed on the surface. The sample presents low roughness of about 1.5 nm and displays well-defined terraced structure with molecular steps close to 2 nm, comparable with the length of C4-NT4N molecule ^[2]. At high deposition rate (Figure 3.8 b) the sample presents a roughness of about 2.5 nm and a morphology characterized by the coexistence of small grains with a later size lower than 100 nm and tridimensional structure on the surface. The thin-film realized by thermal sublimation shows a very high roughness, more than 10nm, characterized by larger grains and tridimensional grain-like structures (Figure 3.8 c). It is interesting to note that the same crystalline phase (phase B) obtained by two deposition technique presents a different morphology. Both the sample show tridimensional aggregates but they are less abundant in the case of the film realized by SuMBD. Moreover SuMBD enables to

obtain a more flat surface with smaller grains. The new phase X, instead, shows a completely different film morphology, with a quasi-2D growth.

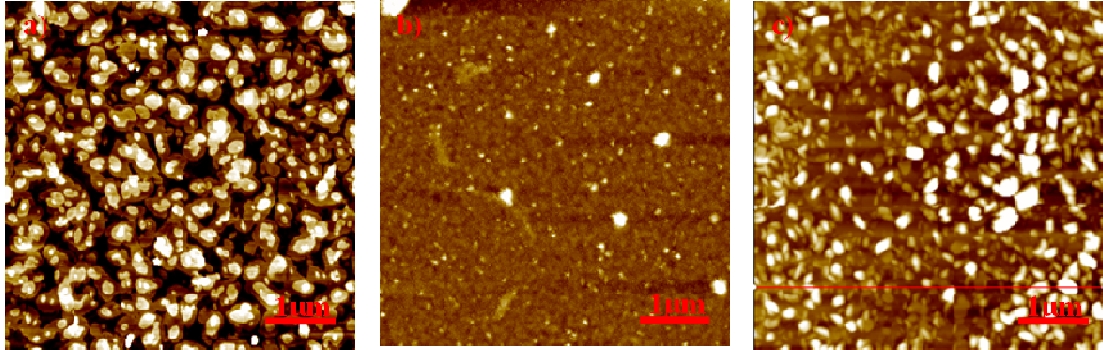


Figure 3.8 AFM image ($5 \mu\text{m} \times 5 \mu\text{m}$ area) of C4-NT4N deposited on Si/SiO₂/HMDS by SuMBD at low rate (a) and high rate (b). AFM image ($5 \mu\text{m} \times 5 \mu\text{m}$ area) of C4-NT4N deposited Si/SiO₂/HMDS by thermal sublimation (c).

Figure 3.9 shows the electrical characteristics of the NT4N based OFETs. Using the bottom-contact configuration, FET behavior for the new phase X was demonstrated.

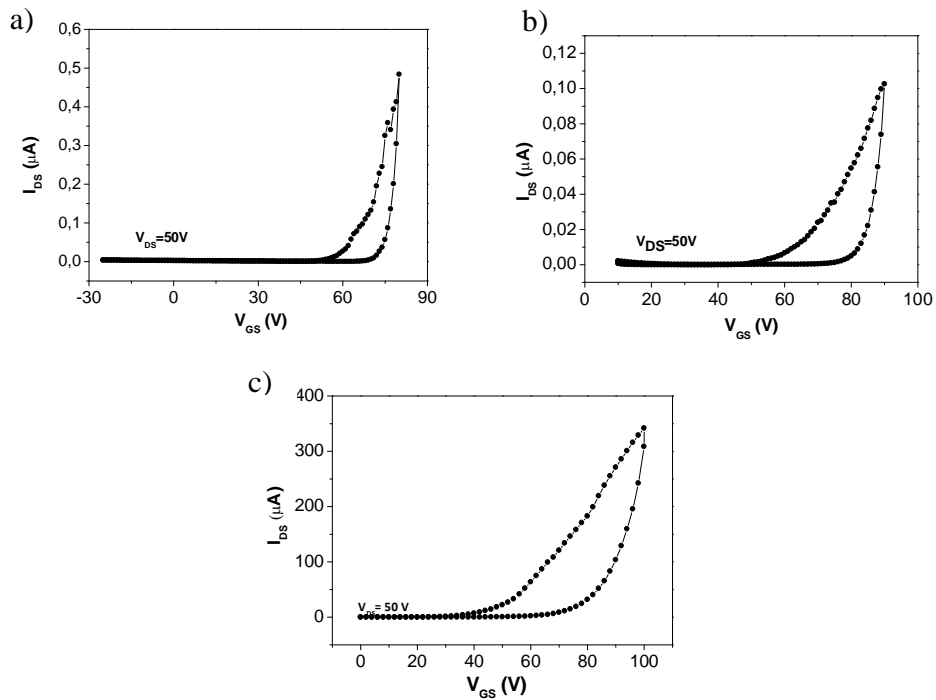


Figure 3.9 N-type transfer saturation curves of BC/BG C4-NT4N based OFET fabricated by SuMBD at 0.1 nm/min (a) and 0.6nm/min. N-type transfer saturation curve of BC/BG C4-NT4N based OFET fabricated by thermal sublimation at 0.6nm/min (c).

The specific molecular arrangement adopted in phase X, revealed by both XRD and PL analysis, leads to different electrical performance with respect to phase B. A maximum mobility of about $10^{-4} \text{ cm}^2\text{V}^{-1}\text{s}^{-1}$ was obtained in n-type polarization but no field-effect in p-type polarization was observed. Devices fabricated at high deposition rate present an ambipolar behavior with unbalanced charge mobilities, as expected from phase B, with electron and hole mobility of $10^{-5} \text{ cm}^2\text{V}^{-1}\text{s}^{-1}$ and $10^{-6} \text{ cm}^2\text{V}^{-1}\text{s}^{-1}$, respectively. Interestingly, deposition by thermal sublimation, although presenting the same crystal packing (phase B), shows mobility values two orders of magnitude higher with respect to the values obtained by SuMBD in the same device architecture (see Table 3.1). Since the molecular structure is the same, the difference in electrical performance could be ascribed to the different film morphology. In the case of phase X which shows a more 2D morphology with well-connected islands a good charge mobility would have been expected [30], but, counter intuitively, the OFET realized by thermal sublimation, which presents a tridimensional growth mode and a high roughness, shows higher mobility with respect to the device realized by SuMBD. All the devices fabricated present bias stress effect, in particular the threshold voltage $|V_{\text{th}}|$ shifts toward higher values upon sweeping the gate voltage, however the initial value is recovered after the measurements. The transfer curves show large clockwise hysteresis, it could be connected with the use of Si/SiO₂ as dielectric. Although the surface was functionalized with a SAM, trapping phenomena are not completely prevented.

Table 3.1 Electrical parameters for BC/BG C4-NT4N based device.

Device	$\mu_e [\text{cm}^2\text{V}^{-1}\text{s}^{-1}]$	$V_t^e [\text{V}]$	$\mu_h [\text{cm}^2\text{V}^{-1}\text{s}^{-1}]$	$V_t^h [\text{V}]$	$I_{\text{on}}/I_{\text{off}}$
SuMBD low rate(phaseX)	1.0E-04	39/55	-	-	10^4
SuMBD high rate(phaseB)	1.0E-05	52/57	2.0E-06	(-35/-38)	10^4
Thermal sublimation(phaseB)	4.5E-02	57/61	6.7E-04	(-71/-73)	10^5

LCW

Previous studies [5] carried out by our group demonstrated that drop-casting from toluene enables the formation of NT4N polymorph A. However, this deposition technique does not allow to obtain a continuous and homogeneous film necessary for OFET fabrication. In order to verify the possibility to fabricate an OFET based on NT4N in phase A, the more soluble C6-NT4N derivative was used and LCW was chosen as deposition

technique. The potentiality of this technique in realizing good pattern with oligothiophene derivatives has been already demonstrated ^[31]. Differently from previous publications, in which the deposition was carried out in air ^[32], this time the overall device was realized under controlled atmosphere in order to prevent degradation phenomena and to optimize the charge transport properties. All the fabrication steps were implemented in a glovebox that ensures levels of oxygen and water below 0.1 ppm. It is worth to note that working in a controlled atmosphere is fundamental for the realization of NT4N based device, indeed electrical characteristics were recorded only when OFETs fabricated inside the glovebox.

In the case of LCW technique, a direct comparison with the benchmark top contact/bottom gate transistor configuration was possible. Since the solvents used in typical wet deposition techniques dissolve the PMMA, the polymeric dielectric was replaced by Cytop, a perfluorinated polymer that ensures the solvent orthogonality. Two different protocols of fabrication were adopted. Since deposition from toluene does not ensure the formation of a pattern connecting source and drain electrodes (Figure 3.10), anisole and 1,2 dichlorobenzene were chosen. The first protocol exploits anisole at 80 °C, the second employs 1,2 dichlorobenzene at room temperature.

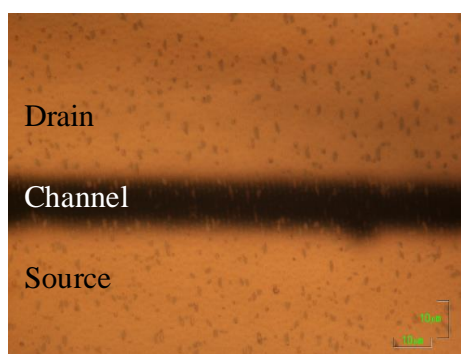


Figure 3.10 TC/BG C6-NT4N based device realized by LCW from toluene, no field effect conduction was recorded.

Figure 3.11 shows optical and AFM image of C6-NT4N based OFET realized with the first protocol. The temperature was chosen in order to enhance the solubility and allow the formation of long-range molecular ordered stripes. The deposited nanostructured films exhibit parallel stripes replicating the orientation and the pitch (1 μ m) of the mold. The AFM characterization clearly shows the absence of a continuous film between the stripes, which have an average height of about 100 nm. A statistical analysis of large

area of printed stripes shows that about 20% of the device channel is covered by stripes effectively connected.

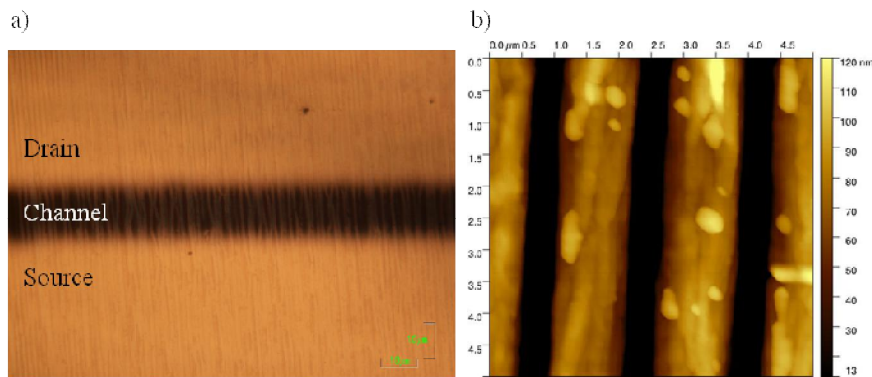


Figure 3.11 TC/BG C6-NT4N based OFET realized by LCW from anisole at 80 °C: optical (a) and AFM (b) image.

XRD and PL characterizations on the device realized according to the first protocol (Figure 3.12) highlight the presence of a unique polymorph, phase B. This could be induced by the annealing step at 80 °C implemented in the fabrication protocol, indeed a phase conversion from phase A to phase B was demonstrated after a thermal annealing at high temperature [5].

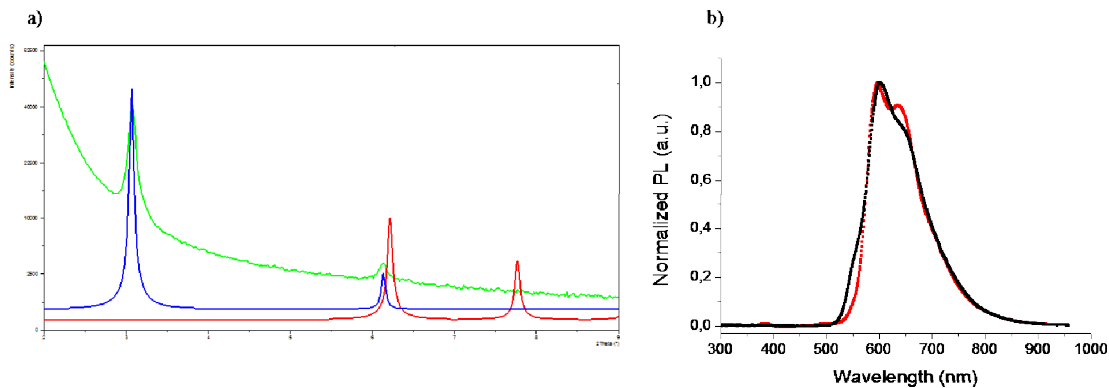


Figure 3.12 (a) X-ray spectrum of C6-NT4N deposited on Cytop by LCW from anisole (green line), theoretical X-ray spectra of C6-NT4N phase A (red line) and phase B (blue line) are reported as comparison. (b) PL spectrum ($\lambda_{ex} = 325$ nm) of C6-NT4N deposited on Cytop by LCW from anisole (red line), PL spectrum of C6-NT4N thin-film by thermal sublimation (phase B) (black line) is reported for comparison.

The second protocol employs 1,2 dichlorobenzene at room temperature, indeed preliminary tests highlight the higher solubility of C6-NT4N in chlorinated solvents also at lower temperature. Interestingly, for this deposition, XRD analysis show the presence

of little amount of phase A coexisting with the more abundant phase B. The XRD pattern (Figure 3.13 a) displays a peculiar profile with a doublet revealing the coexistence of two different polymorphs.

Images collected by Confocal Laser Scanning Microscope (Figure 3.13 b) show a pattern of ordered parallel stripes replicating the pitch of the mold. The samples are characterized by large ordered domains. The localized PL spectra were collected in different areas of the nanostructured film, but only phase B was identified (Figure 3.13 c). It is important to underline that the sensitivity of the PL technique is correlated not just with the amount of material but also with the PL quantum yield of each phase. Thus, the impossibility to reveal phase A by optical technique could be connected to a difference in quantum yields of the two polymorphs.

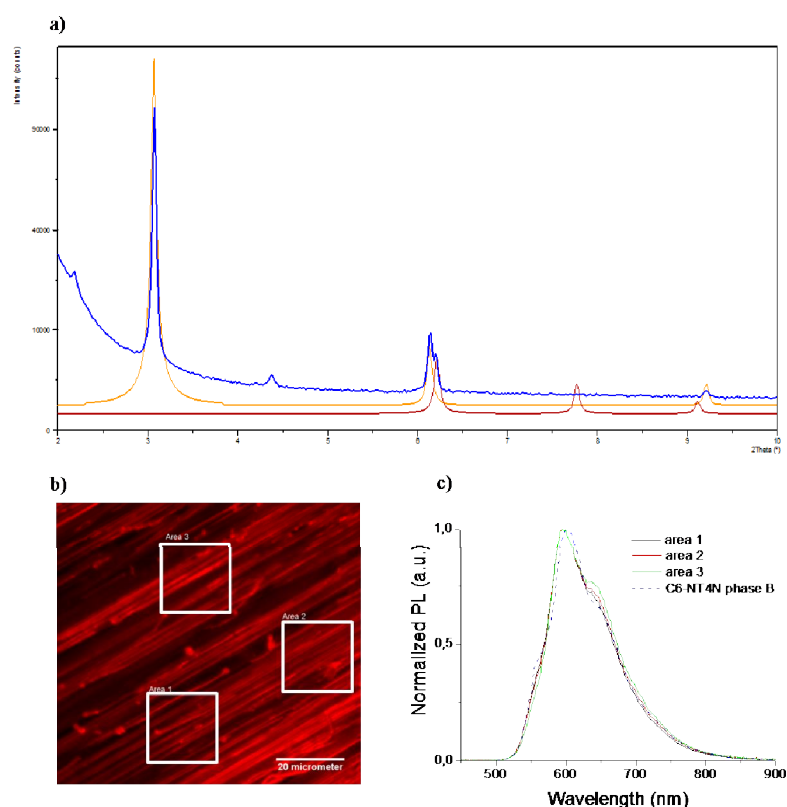


Figure 3.13 (a) X-ray spectrum of C6-NT4N deposited on Cytop by LCW from 1,2 dichlorobenzene (blue line), theoretical X-ray spectra of C6-NT4N phase A (red line) and phase B (orange line) are reported as comparison. (b) Confocal fluorescence image and (c) localized emission spectra ($\lambda_{ex} = 405$ nm) of C6-NT4N deposited on Cytop by LCW from 1,2 dichlorobenzene.

Regardless the discrimination of crystal phase involved in the transport, we underline that we succeeded in achieving the objective of this study, given that we demonstrate

field-effect charge transport in field-effect condition for NT4N derivative deposited by a wet technique.

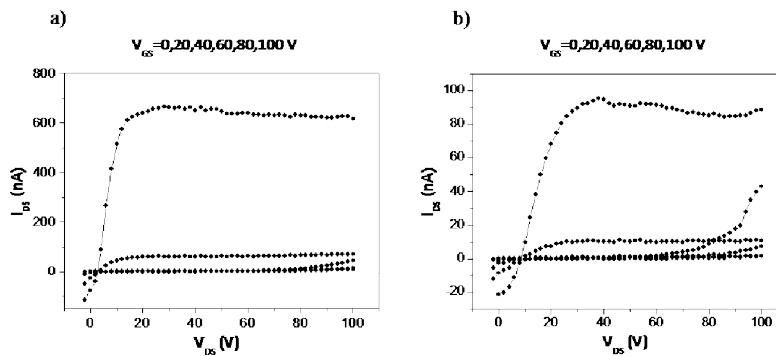


Figure 3.14 Multiple output characteristics of TC/BG OFET based on micro-strips of C6-NT4N printed perpendicularly to the electrodes by LCW from anisole solution (a) and from 1,2 dichlorobenzene solution (b).

Although the electrical performance and the drain currents observed are very low, the output characteristics curves (Figure 3.14) present superimposition of standard saturation behavior for one charge carrier and a superlinear current increase due to injection of the other charge carrier, indication of the typical ambipolar transport behavior expected for phase B.

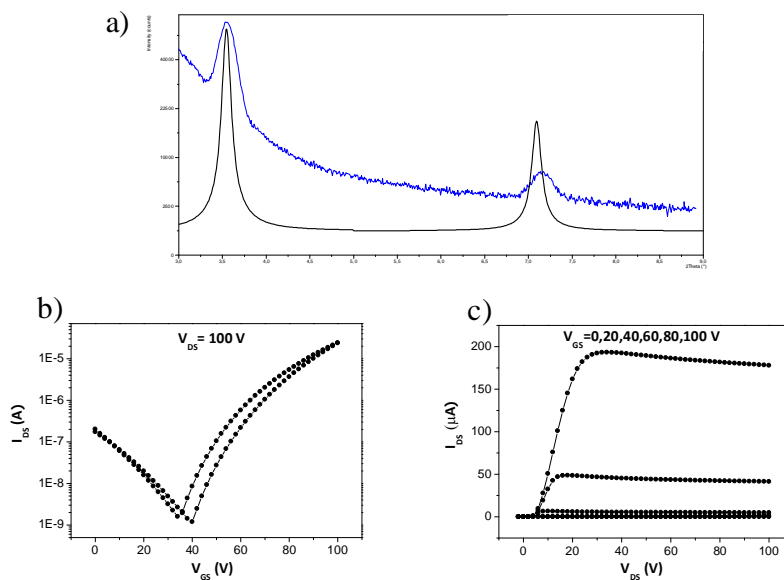


Figure 3.15 X-ray spectra of NT4N thin-film deposited on Cytop by thermal sublimation (a). Electrical characterization performed on single-layer TC/BG OFET based on 75 nm of NT4N on Cytop: (b) n-type transfer saturation curve, (c) n-type multiple output curves.

A device onto glass/ITO using 450 nm of Cytop as dielectric layer was realized by thermal sublimation as reference. XRD analysis shows crystal packing compatible with phase B (Figure 3.15 a), as in the case of PMMA dielectric. Moreover, the electrical performance of Cytop-based device are comparable with the PMMA-based ones (Figure 3.15 b and c). In Table 3.2 the electrical parameters for the TC/BG device realized on Cytop are reported. All the device present ambipolar behaviour with unbalanced mobilities. In the case of the device realized from 1,2 dichlorobenzene a decrease in the n-type mobility was observed. In order to understand if it is connected to the presence of a different polymorph, theoretical calculations are currently ongoing to correlate the crystal packing and the charge mobility in NT4N.

Table 3.2 Electrical parameters for TC/BG NT4N based device on Cytop.

Device	μ_e [$\text{cm}^2\text{V}^{-1}\text{s}^{-1}$]	V_t^e [V]	μ_h [$\text{cm}^2\text{V}^{-1}\text{s}^{-1}$]	V_t^h [V]
LCWfrom anisole (phase B)	2.4E-03	62	1.0E-05	-56
LCW from 1,2dichlorobenzene (phase B+A)	4.4E-04	60	2.7E-05	-64
Thermal sublimation (phase B)	2.0E-01	57	2.2E-03	-68

3.4 Conclusions

The small-molecule semiconductor NT4N displays charge transport capability, polymorphism and electroluminescence. These features enable the successful application of this material as active layer in integrated charge transport based organic devices such as ambipolar single layer OFETs and OLETs. In this study the correlation between processing, structure and function in NT4N was investigated. Giving the possibility of NT4N derivatives to be processed by both dry and wet techniques, polymorphism was probed and revealed by choosing different deposition techniques, i.e. thermal sublimation, SuMBD and LCW. Morphological, structural, optical and electrical characterizations enabled to correlate the process of deposition with the molecular packing, the film morphology and the device electrical performance. Given the different specificities of the techniques in terms of thermodynamic and kinetic regimes, we succeeded in controlling the solid-state phases of the NT4N layer comprising the OFET devices. Three polymorphs have been found, two already known and a new phase

studied here for the first time. Indeed, the use of SuMBD permits to identify a new polymorph capable to transport in field-effect geometry while LCW enable the formation of two different phases. For the first time field-effect charge transport in NT4N nanostructured films deposited by wet technique was shown. Comparing all the device configurations and the deposition techniques investigated, top contact/bottom gate OLET by thermal sublimation is the best-performing device and represents the benchmark device that can be implemented as optoelectronic component in more complex photonic systems.

References

- [1] M. Muccini, S. Toffanin, *Organic Light-Emitting Transistors: Towards the Next Generation Display Technology*, Ed. Wiley-Science, Wise Co-Publication, **2016**.
- [2] M. Melucci, M. Zambianchi, L. Favaretto, M. Gazzano, A. Zanelli, M. Monari, R. Capelli, S. Troisi, S. Toffanin, M. Muccini, *Chem. Commun.* **2011**, *47*, 11840.
- [3] M. Melucci, L. Favaretto, M. Zambianchi, M. Durso, M. Gazzano, A. Zanelli, M. Monari, M. G. Lobello, F. De Angelis, V. Biondo, G. Generali, S. Troisi, W. Koopman, S. Toffanin, R. Capelli, M. Muccini, *Chem. Mater.* **2013**, *25*, 668.
- [4] M. Melucci, M. Durso, C. Bettini, M. Gazzano, L. Maini, S. Toffanin, S. Cavallini, M. Cavallini, D. Gentili, V. Biondo, G. Generali, F. Gallino, R. Capelli, M. Muccini, *J. Mater. Chem. C* **2014**, *2*, 3448.
- [5] L. Maini, F. Gallino, M. Zambianchi, M. Durso, M. Gazzano, K. Rubini, D. Gentili, I. Manet, M. Muccini, S. Toffanin, M. Cavallini, M. Melucci, *Chem. Commun.* **2015**, *51*, 2033.
- [6] J. Soeda, T. Uemura, Y. Mizuno, A. Nakao, Y. Nakazawa, A. Facchetti, J. Takeya, *Adv. Mater.* **2011**, *23*, 3681.
- [7] M. Mas-Torrent, C. Rovira, *Chem. Rev.* **2011**, *111*, 4833.
- [8] D. Fox, M. M. Labels, A. Weissberger, Eds. , *Physics and Chemistry of the Organic Solid State*, Interscience Publishers, London, **1965**.
- [9] J. Bernstein, *Polymorphism in Molecular Crystals*, Clarendon Press, Oxford, **2002**.
- [10] A. J. Cruz-Cabeza, J. Bernstein, *Chem. Rev.* **2014**, *114*, 2170.
- [11] A. Troisi, *Chem. Soc. Rev.* **2011**, *40*, 2347.

- [12] W.-Y. Chou, M.-H. Chang, H.-L. Cheng, Y.-C. Lee, C.-C. Chang, H.-S. Sheu, *J. Phys. Chem. C* **2012**, *116*, 8619.
- [13] A. Moser, I. Salzmann, M. Oehzelt, A. Neuhold, H.-G. Flesch, J. Ivanco, S. Pop, T. Toader, D. R. T. Zahn, D.-M. Smilgies, R. Resel, *Chem. Phys. Lett.* **2013**, *574*, 51.
- [14] T. Siegrist, C.Kloc, R. A. Laudise, H. E. Katz, R. C. Haddon, *Adv. Mater.* **1998**, *10*, 379.
- [15] K. Walzer, T. Fritz, K. Leo, *Surf. Sci.* **2006**, *600*, 2064.
- [16] L. A.Stevens, K. P. Goetz, A. Fonari, Y. Shu, Rachel M. Williamson, V. C. Bredas, Jean-Luc, Oana D. Jurchescu, Gavin E. Collis, *Chem. Mater.* **2015**, *27*, 112.
- [17] S. Iannotta, T. Toccoli, *J. Polym. Sci. Part B Polym. Phys.* **2003**, *41*, 2501.
- [18] F. Chiarella, T. Toccoli, M. Barra, L. Aversa, F. Ciccullo, R. Tatti, R. Verucchi, S. Iannotta, A. Cassinese, F. Chiarella, T. Toccoli, M. Barra, L. Aversa, F. Ciccullo, R. Tatti, R. Verucchi, *Appl. Phys. Lett.* **2014**, *104*.
- [19] Y. Wu, T. Toccoli, N. Koch, E. Iacob, A. Pallaoro, P. Rudolf, S. Iannotta, *Phys. Rev. Lett.* **2007**, *98*, 1.
- [20] M. Castriota, E. Cazzanelli, S. Forti, G. Tarabella, T. Toccoli, K. Walzer, S. Iannotta, *J. Phys. Chem. C* **2010**, *114*, 7038.
- [21] Massimiliano Cavallini, C. Albonetti, F. Biscarini, *Adv. Mater.* **2009**, *21*, 1043.
- [22] M. Cavallini, D. Gentili, P. Greco, F. Valle, F. Biscarini, *Nat. Protoc.* **2012**, *7*, 1668.
- [23] M. Cavallini, P. Stoliar, M. Surin, P. Leclé, R. Lazzaroni, D. W. Breiby, J. W. Andreasen, M. M. Nielsen, P. Sonar, A. C. Grimsdale, K. Mu, *Nano Lett.* **2005**, *5*, 2422.
- [24] F. Chiarella, M. Barra, A. Carella, L. Parlato, E. Sarnelli, A. Cassinese, *Org. Electron.* **2016**, *28*, 299.
- [25] M. Barra, D. Viggiano, P. Ambrosino, F. Bloisi, F. V. Di Girolamo, M. V. Soldovieri, M. Tagliatela, A. Cassinese, *Biochim. Biophys. Acta - Gen. Subj.* **2013**, *1830*, 4365.
- [26] L.-L. Chua, J. Zaumseil, J.-F. Chang, E. C.-W. Ou, P. K.-H. Ho, H. Sirringhaus, R. H. Friend, *Nature* **2005**, *434*, 194.
- [27] M. C. Petty, *Molecular Electronics: From Principles to Practice*, John Wiley &

Sons Ltd., Chichester, **2007**.

- [28] M. Pope, C. E. Swenberg, *Electronic Processes in Organic Crystals*, Oxford University Press, **1982**.
- [29] M. A. Loi, E. Da Como, F. Dinelli, M. Murgia, R. Zamboni, F. Biscarini, M. Muccini, *Nat. Mater.* **2005**, *4*, 81.
- [30] F. Dinelli, M. Murgia, P. Levy, M. Cavallini, F. Biscarini, D. M. De Leeuw, *Phys. Rev. Lett.* **2004**, *92*, 116802.
- [31] M. Durso, D. Gentili, C. Bettini, A. Zanelli, M. Cavallini, F. De Angelis, M. G. Lobello, V. Biondo, M. Muccini, C. Raffaella, M. Melucci, *Chem. Commun.* **2013**, *49*, 4298.
- [32] D. Gentili, M. Durso, C. Bettini, I. Manet, M. Gazzano, R. Capelli, M. Muccini, M. Melucci, M. Cavallini, *Sci. Rep.* **2013**, *3*.

Chapter 4

Anthracene-based molecular emitters for non-doped deep-blue organic light emitting transistors

4.1 Introduction

The synthesis of a single material capable of providing both high current density and intense electroluminescence in single-layer field-effect devices is a very challenging task. In most cases, organic semiconductors with high carrier mobility due to the strong intermolecular π stacking suffer from luminescence quenching in the solid state in correlation to the singlet fission or exciton quenching. The limited number of efficient electroluminescent organic small molecules with good ambipolar mobility values is thus a detrimental factor in achieving high-performance OLETs based on a single active layer. In single-layer OLET device configuration, Adachi et al. introduced the use of a bis(styryl)biphenyl derivative as a blue-emitting ambipolar organic semiconductor ^[1]. The same group reported a blue-emitting OLET with an external quantum efficiency (EQE) up to 0.2% by implementing a fluorene asymmetric derivative in a single-layer bottom contact/bottom gate (BC/BG) OLET by exploiting the two-color electrode configuration ^[2]. However, using a single material for transporting hole carriers and emitting light leads to poor device performance in terms of hole mobility and source-drain current (around 10^{-6} cm² V⁻¹ s⁻¹ and 2 mA, respectively). Moreover, the emitted light intensity was observed to increase with the gate voltage up to a maximum and to decrease by further increasing the gate voltage and corresponding current. This evidence was correlated with the use of a single-layer device in a BC/BG configuration. In this view, the use of a multilayer architecture, where each layer is optimized according to its

specific function leads to a better performance^[3]. While a single-layer OLET requires an active material showing the best trade off between high charge transport capability and high electroluminescence, a multilayer configuration gives the possibility to overcome this limitation and optimize each feature in a different layer. An interesting device platform based on organic light-emitting transistor technology consists in implementing a bilayer film comprising a field-effect charge-transport layer and a light-emitting layer as a device active region. The bilayer configuration allows the decoupling of the region of high charge-carrier density from the light emission region so that the processes such lateral charge transport, exciton formation and radiative deactivation can be optimized independently. This architecture enables the investigation and the optimization of emissive materials to be employed as emissive-layer in optoelectronic devices.

The development of efficient emitting organic materials has gained increasing interest in the last decade for their potential applications as emissive layers in organic light emitting devices suitable for full color display fabrication^[4]. In display technology each color is obtained by the combination of the fundamental red, green and blue (RGB) colors and in order to achieve high quality vision experience (quantified by the color gamut) precise color coordinate are required for each fundamental color. The major challenge is the development of a deep, efficient and stable blue. Indeed, blue emission from organic materials undergoes fundamental energetic and electronic constraints, which affect its emission spectrum, efficiency, and molecular structural stability under operational conditions^[5]. Different molecular structures including carbazole-dimesitylborane^[6], and imidazole-p-triphenylamine derivatives^[7], among others, have been implemented so far and tested as blue emitters in both host-guest and single-component emission layers in OLEDs (i.e. metal complexes-free). It is highly preferable to implement a single-component emission layer in a multilayer organic optoelectronic device. The constraints on the HOMO/LUMO level energetic in host-guest system, which guarantee both efficient energy transfer and the intense deep blue emission from the dopants, are, in fact, not easily satisfied in a multilayer/multicomponent OLEDs. Moreover the fabrication process of organic optoelectronic devices is simplified in the case of a single emission layer.

The common motif of the proposed molecular structures in targeting blue emission requirement lies in the reduced π -conjugation extent that prevents red-shifted emission and strong crystallization tendency in films. Anthracene-based materials have emerged

as valuable materials for blue OLEDs realization. In particular, the anthracene core substituted at the 9,10-positions are related to excellent photoluminescence and electroluminescence properties, poorly crystalline film morphology and HOMO/LUMO energy level fine-tunability^{[8][9]}. Kim et al. demonstrated by means of a rationally designed class of anthracene-based emitters that anthracene substitution with bulky substituents provides steric hindrance, which prevents intermolecular interactions and reduces self-quenching effects leading to improved EL performances^{[10][11]}. Recently, the effect of the substitution of anthracene with 2,5-dimethyl-xylene on the optical and morphology properties of the resulting molecular derivatives has been investigated. For the twisted BDNA derivative (Figure 4.1) CIE coordinates of (0.159;0.072) and a maximum external quantum efficiency (EQE) of 5.26% were reported^[10]. The effect of molecular symmetry on the color coordinates and device efficiency was also investigated. Bisanthracene-based donor acceptor type derivatives with symmetric or asymmetric structure have also been developed with the aim of further rigidifying the system to prevent π -conjugation. For the asymmetric BD3 derivative (Figure 4.1) an EQE of 4.2% with CIE color coordinates of (0.15;0.06) was obtained which are close to the CIE coordinates of the high definition standard blue^[12]. According to these structure-design requirements, a new anthracene derivative twisted oligomer combining a rigid anthracene-xylene core with diphenylamine ends 4,40-(anthracene-9,10-diyl)bis(2,5-dimethyl-N,N-diphenylaniline), namely DiPAXA (Figure 4.1), was recently synthesized by the group of Manuela Melucci at CNR-ISOF in Bologna^[13].

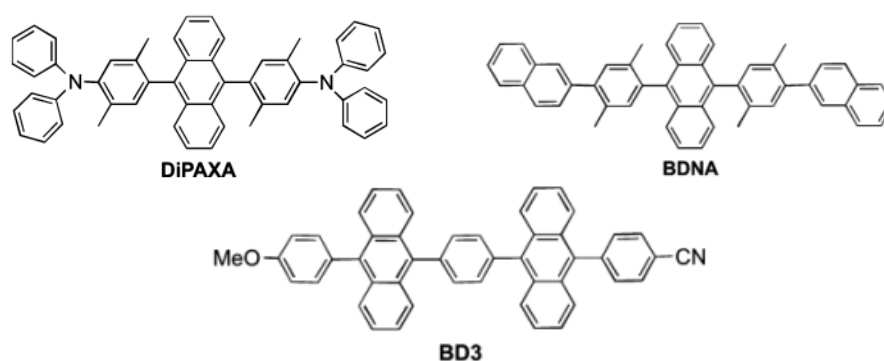


Figure 4.1 Molecular structure of the anthracene derivatives.

The main topic of this work was aiming at studying the optoelectronic properties of the new compound DiPAXA and at comparing them to those of two other anthracene-based materials namely BDNA and BD3. For performing the optoelectronic characterization of

those compounds we integrated them as single-component emitting layer in OLET device platform. A bilayer active region OLET in top contact/bottom gate (TC/BG) configuration was used as a device platform for comparing and screening the three blue emitters as a possible class of materials for OLET fabrication.

4.2 Synthesis

DiPAXA was synthesized starting from 9,10-bis(4-bromo-2,5-dimethylphenyl)anthracene **1** and diphenylamine **2** under Pd catalysis in the presence of NaOtBu as depicted in Figure 4.2. Compound **1** was prepared by nucleophilic addition reaction of anthraquinone and monolithiated dibromoxylene according to the already described procedure^[10]. Differential scanning calorimetry under a nitrogen atmosphere, reveals a melting transition at about 370 °C suggesting a high thermal stability.

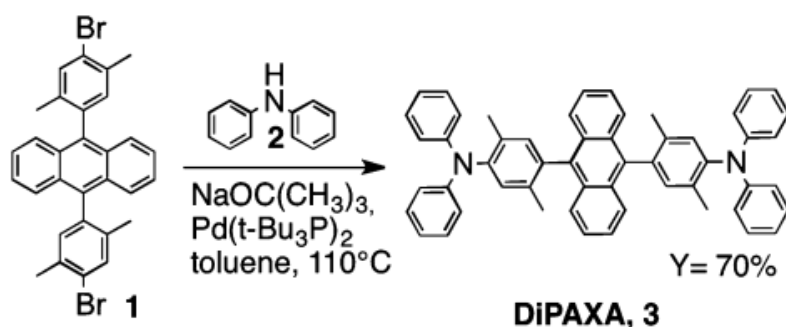


Figure 4.2 Synthetic route to DiPAXA.

4.3 Optoelectronic properties of anthracene derivatives

The optoelectronic properties of the newly synthesized DiPAXA were characterized and compared to those of the already known anthracene based compounds BD3 and BDNA. The three materials were characterized in both solution and solid state (Table 4.1). 10⁻⁵M solution in dichloromethane and thin film (60 nm) deposited on quartz by thermal sublimation in high vacuum at a rate of 6 nm/min were prepared. The absorption spectra (Figure 4.3) of the three materials show the typical vibrational pattern of the anthracene moiety with peaks located at about 340, 350, 380 and 400 nm. The photoluminescence (PL) spectra (Figure 4.3) are broad and unstructured with maximum-emission peaks in the blue range both for DiPAXA and BD3. In particular, DiPAXA presents maximum-emission peaks at 469 and 457 nm for the solution and the thin-film, respectively.

Table 4.1 Optoelectronic data.

Item	BD3	BDNA	DIPAXA
abs ^a (nm)	359,378,399	342,358,378,398	358, 377, 398
abs ^b (nm)	364,384,405	344,360,379,401	359, 380, 401
em ^a (nm)	430, (443)	411,430, 453, 485	469, (418)
em ^b (nm)	(448),480	411, 434, 466, 501	457 (455)
PLQY ^c (%)	20/7	82/50	86/50
HOMO (eV) (theo/exp)	-5.34/-6.01 ^d	-5.25/-5.91 ^e	-5.17/-5.71 ^e
LUMO (eV) (theo/exp)	-2.40/-3.03 ^d	-2.15/-2.88 ^f	-2.26/-2.71 ^f
E _g (eV)	2.98 ^d	3.04 ^g	3.00

^aCH₂Cl₂ solutions, ^bfilm (60nm), ^csolution/film, ^dfrom ^[11], ^eE_{HOMO} = e(4.68+E_{ox}), where E_{ox} was computed vs. SCE, ^fcalculated from the optical band gap. E_g is the optical energy gap, ^gfrom ^[10].

A blue-shift in the main emission peak of about 10 nm is observed in the thin-film PL spectrum. The optical features of the emission profiles highlight not only the fact that the molecule preserves the non-planar configuration in the thin-film, but also the fact that the overall molecular π -conjugation is further reduced possibly due to the increase in steric hindrance as the moieties arrange in the solid state. Differently, BDNA presents structured PL spectra both in the solution and the thin-film. In particular, the thin-film PL spectrum presents at least three clear peaks with a large full width at the half maximum value (around 90 nm). Even though there is almost no Stoke shift in both the solution and the thin-film in the case of BDNA, the emission profile features in the solid state are possibly detrimental to achieving suitable CIE coordinates in the final device. Interestingly, the DiPAXA and the BDNA present similar values of PL quantum yield, namely around 82-86% and 50% in the solution and in the thin-film, respectively, that, in principle, makes them good candidates for device applications. In the case of BD3, instead, the introduction of asymmetric end-substituents results in very low PL quantum yield in solid state, around 7%. From spectroscopic investigation, we can assess that the molecule-design strategy for DiPAXA is effective in achieving deep-blue emitting compounds with high quantum yield in the solid state.

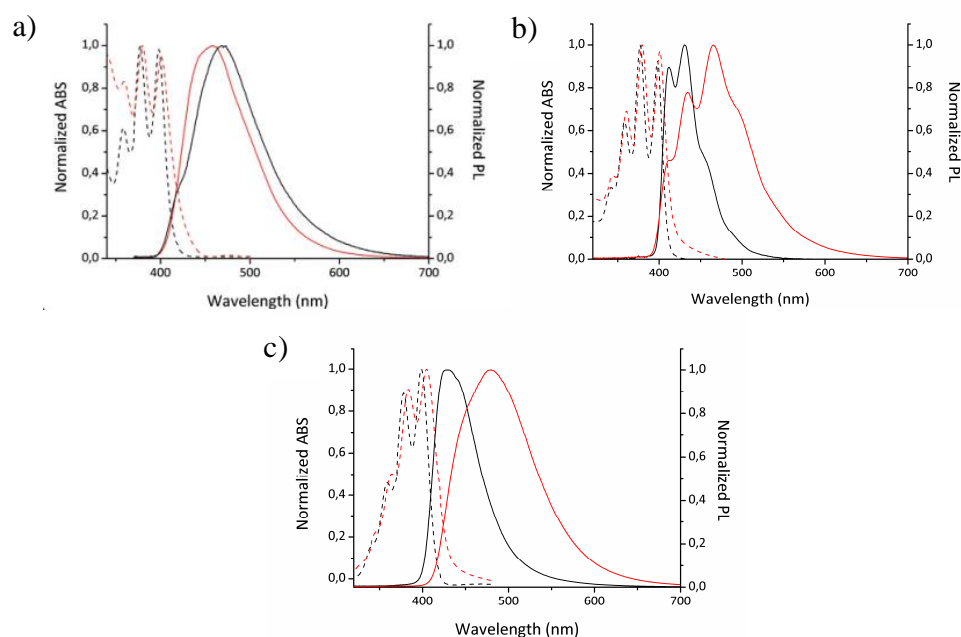


Figure 4.3 Absorption (dotted lines) and emission (solid lines) spectra in solution (black lines) and neat film (red lines) of DiPAXA (a), BDNA (b) and BD3 (c).

Theoretical calculations by using the density functional theory (DFT) B3LYP/6-311+G* method were performed to calculate HOMO/LUMO energy level values and frontier orbital energy distributions. The results are shown in Figure 4.4. The calculated molecular geometry for DiPAXA shows an almost orthogonal arrangement between the anthracene and the xylene moiety. Calculations also show that while the HOMO electron density is mainly localized on the xylene-diphenyl amine arm, the LUMO density is mainly located on the anthracene core. The non-planar overall configuration limits the degree of conjugation, which positively affects both the emission feature and the crystallization capability. An optical gap $S_0 - S_1$ of 2.90 eV (427 nm) is computed for the molecule in a vacuum.

Cyclic voltammetry (CV) experiments were carried out in order to obtain the experimental values of HOMO and LUMO energy levels. A value of -5.71 eV was calculated from experiments carried out both in CH_2Cl_2 and THF solutions, revealing that this compound is reversibly oxidized with $E_{1/2} = +0.56 \text{ V vs. Fe}^+/\text{Fe}$. This value, lower with respect to both BD3 and BDNA, is consistent with the electron-donating mesomeric effect induced by the nitrogen atom conjugated to the anthracene moiety. Unfortunately, any attempts to compute the LUMO energy level from CV traces failed.

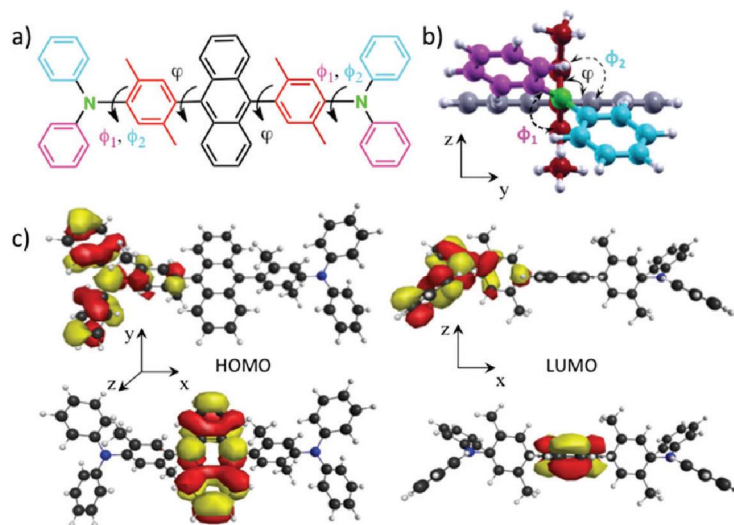


Figure 4.4 (a) Molecular sketch and (b) optimized geometry of DiPAXA with torsional angles ϕ between anthracene and xylene and ϕ_1 between xylene and diphenylamine $\phi_1 = 117^\circ$, $\phi_2 = 126^\circ$, and $\phi = 90^\circ$. (c) DiPAXA frontier molecular orbitals (HOMO left column, and LUMO right column).

4.4 Fabrication and characterization of unipolar bilayer OLET devices

Organic light-emitting transistors were fabricated on glass/ITO substrates where ITO works as a gate electrode and PMMA (450 nm) is used as a gate dielectric. The organic active region consists of a stacked bilayer formed by 45nm of 2,7-dioctyl[1]benzothieno[3,2-b][1]benzothiophene (C8-BTBT) as p-type semiconductor in direct contact with the dielectric layer and a compact thin film made of anthracene derivative (60 nm) as emissive layer (Figure 4.5 a). The material C8-BTBT was chosen for the high hole mobility ^{[14][15]}. In order to optimize the charge-transport layer, preliminary tests on a single-layer C8-BTBT based device were carried out. The thickness of 45 nm was adopted as a good compromise between the thickness and the values of charge mobility, in particular, a charge mobility value of about $3 \text{ cm}^2\text{V}^{-1}\text{s}^{-1}$ was measured. The bilayer configuration realized leads to an unipolar field-effect transistor in which only the positive charge carriers can move inside the device through the p-type transport layer. The electrons remain confined at the injection electrode so that the recombination zone is expected to be under the drain electrode. Saturation transfer curves ($V_{\text{DS}} = -100 \text{ V}$) are shown in Figure 4.5 b as well as the measured emitted optical power and calculated EQE. As expected, the devices behave only as a p-type transistor, with C8-BTBT dominating the field-effect transport within the device.

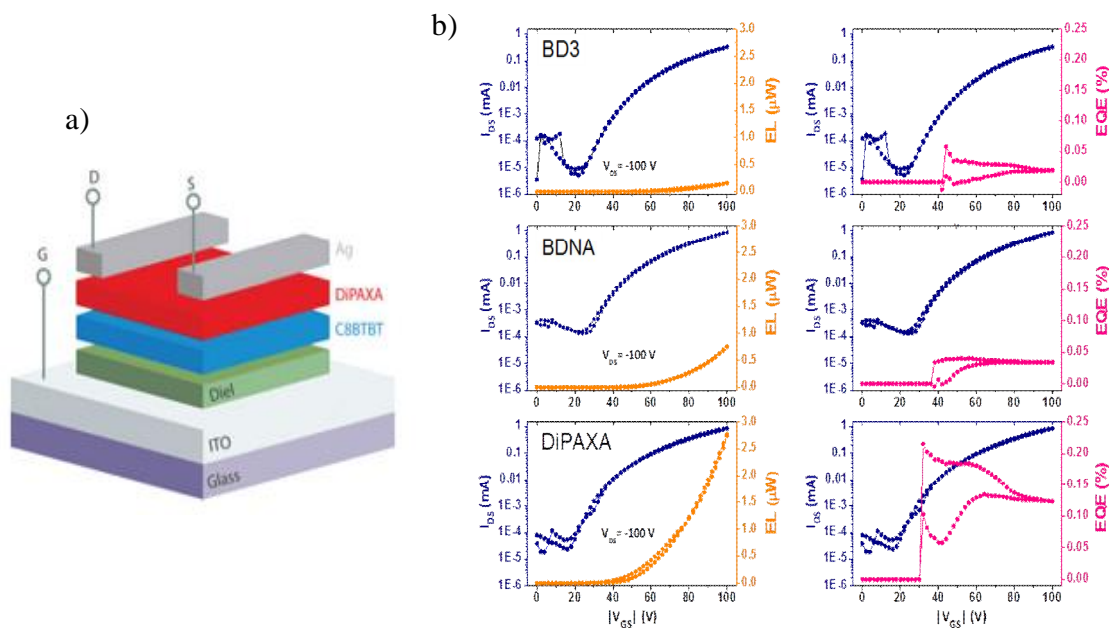


Figure 4.5 (a) Schematic representation of the organic light-emitting transistor in bilayer configuration. (b) Saturation transfer curves with corresponding optical power (left side) and external quantum efficiency (right side) of BD3, BDNA and DiPAXA in the same bilayer configuration.

The electrical properties are reported in Table 4.2. All the transistors show a value of the I_{on}/I_{off} ratio of approximately $10^4 - 10^5$. BD3 based OLETs present worse electrical performance with respect to BDNA and DiPAXA based devices. Interestingly using DiPAXA as emissive layer a maximum output optical power of about 2.75 mW was reached, higher with respect to the other materials. Figure 4.5 b shows the external quantum efficiency, which correlates the number of available charge carriers with the number of emitted photons upon radiative recombination. In the limit $V_{DS} = V_{GS} = -100$ V (unipolar condition) the value of EQE for the DiPAXA based device is approximately 0.125%, about one order of magnitude larger than the corresponding values obtained for the other anthracene-based materials in the same device configuration. Despite the different device architectures and materials used, this value of efficiency resides within the same range for other bilayer OLET devices ^{[16][17]}.

Prior to optical characterization carried out in the atmosphere, as-fabricated devices were encapsulated inside the glovebox using a glass coverslip and an ultraviolet-cured epoxy sealant. A getter (Dryflex, provided by SAES-GETTERS) was also used to prevent any deterioration of the sample. Figure 4.6c shows optical images of DiPAXA OLETs while mounted on a sample holder in their ON-state for one or multiple devices.

Table 4.2 Summary of the electrical and optical properties of TC/BG bilayer OLETs fabricated.

	$ I_{DS-max} $ (μA)	μp ($cm^2V^{-1}s^{-1}$)	$ V_{th, p} $ (V)	Elmax (μW)	EQE@100V (%)	CIE coord. (X,Y)
BD3	329	0.15	41.7	0.16	0.019	(0.19, 0.19)
BDNA	880	0.46	34.0	0.76	0.034	(0.20, 0.23)
DiPAXA	860	0.32	25.8	2.75	0.125	(0.18, 0.21)

The normalized electroluminescence (EL) spectrum of one of the representative DiPAXA-OLETs biased at $V_{DS} = V_{GS} = -100$ V shows a broad peak (FWHM = 90 nm) centred at around 470 nm. From the device EL spectrum, it was also possible to determine the color coordinates of our organic light emitting transistors (Figure 4.5 b), which are $x = 0.18$ and $y = 0.21$. The coordinates of the BD3 and BDNA are also reported for comparison. It can be seen that the emission of the DiPAXA based device is characterized by a deeper blue component, thus leading to a blue emission closer to currently available standards (PAL, NTSC) as it was expected from the optical spectroscopic investigation ^[18]. The microscopy image showing in more detail the channel area of an individual device is displayed in Figure 4.5 d. It can be seen that when the OLET is lit, the light emission is located below the drain electrode, as expected for an unipolar transistor ^[19].

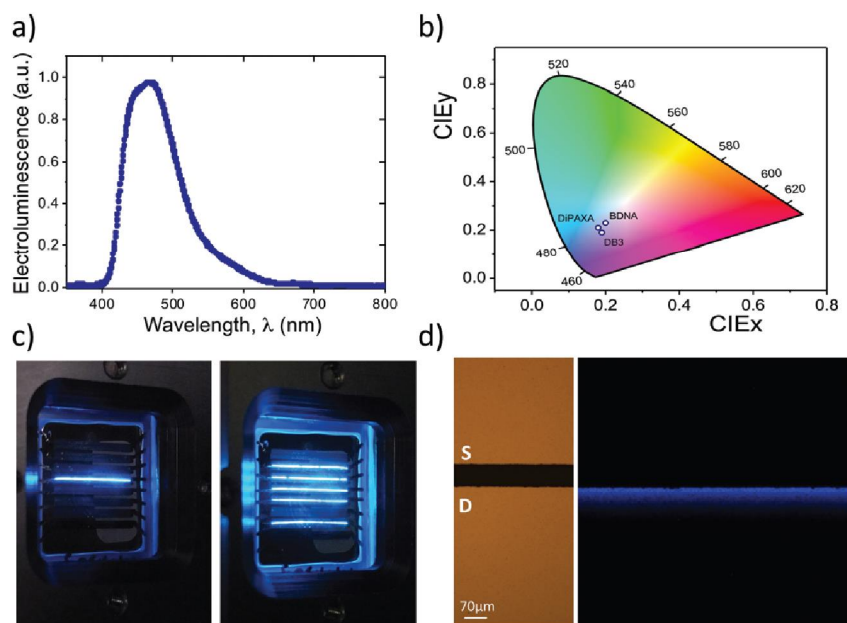


Figure 4.6 (a) Normalized electroluminescence (EL) spectra of one of our representative DiPAXA-OLETs with (b)XY color map plane (CIE standard) indicating the color coordinates of various emitting materials analyzed in this work (DiPAXA) (0.18; 0.21). The CIE map has been adapted from an online available source file from OriginLabs. Color coordinates of BDNA and BD3 corresponding devices are also reported for reference. (c) Optical images of one of our DiPAXA organic light-emitting transistors where one or multiple individual linear devices are in their ON-state. (d) Microscopy image on one of our representative DiPAXA OLETs in the (left) OFF- and (right) ON state, showing the localization of the light emission below the drain electrode.

Despite a similar PLQY value and almost comparable mobility values (see Tables 4.1 and 4.2), the EQE measured for the DiPAXA device was one order of magnitude higher than that of the BDNA based device. A possible explanation for the different behaviour can rely on the material/electrode energy level match. The energy level diagrams (Figure 4.7) show that DiPAXA has a better energy alignment with C8-BTBT in comparison with BDNA, given that the DiPAXA HOMO level is higher than that of C8-BTBT (about 0.2 eV). This clearly indicates that, thanks to this energy mismatch, in the DiPAXA based device holes are accumulated at the emitters/C8-BTBT interface (emitter side). Conversely, in the case of BDNA (and even worse in the case of BD3) there is no energy mismatch (and for BD3 the mismatch is even inverted) and holes are likely to be preferentially accumulated at the p-type semiconductor. Regarding electrons, in all the device structures the LUMO energy barrier hinders the charge percolation into

the C8-BTBT layer. By virtue of the previous considerations, excitons can be formed efficiently only in DiPAXA based devices, given the coexistence of charges of opposite signs in the emissive layer. This possible light-formation mechanism is corroborated by the one order-of-magnitude higher optical power measured in DiPAXA based OLETs with respect to BDNA and DB3.

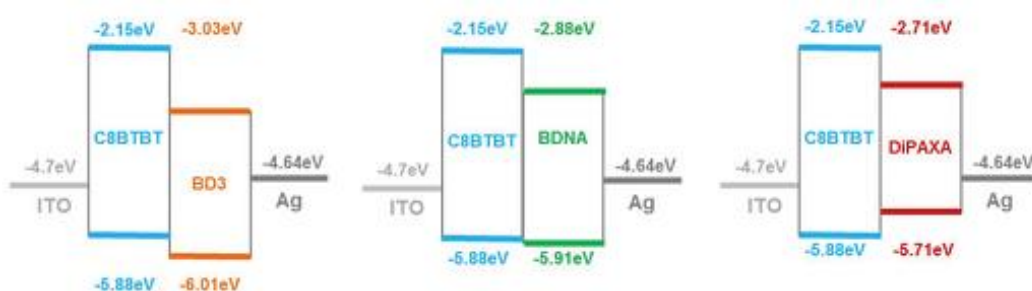


Figure 4.7 Schematic representation of the experimental energy level diagrams of the OLET device for BD3, BDNA and DiPAXA materials.

4.5 Conclusions

The implementation of a multilayer heterostructure comprising a charge-transport layer and a light-emitting layer, enabled to overcome the poor field-effect charge mobility often associated with high electroluminescence materials. We engineered a bilayer configuration in which was possible to demonstrate the suitability of twisted anthracene molecular emitters as a class of blue emitting material for OLET realization. In collaboration with the CNR-ISOF a new anthracene based material namely DiPAXA was synthesized and characterized in bilayer-configuration device. The performance of DiPAXA was compared to that of two other anthracene-based materials namely BDNA and BD3 already used for OLED applications. All the compounds demonstrated light emission correlated with field-effect charge transport conditions and, in particular, DiPAXA showed slightly deeper blue electroluminescence and higher external quantum efficiency with respect to BDNA and BD3.

The use of the bilayer configuration gave us the possibility to implement a simple and reliable device platform for comparing and screening different emitting materials. However, it does not offer any control on the exciton quenching and photon losses due to the fact that charge recombination and light emission are located in the proximity of the charge-collecting electrode. Excitons interact with accumulated charges and the

metal electrode, whereas photons are absorbed by the contacts. The implementation of these materials in a trilayer architecture where both hole and electron currents are maximized and balanced could give the possibility to obtain better optoelectronic performance. Nevertheless a trilayer configuration requires energetic compatibility between the materials forming the heterostructure and the morphology of the superimposed films must allow the formation of a continuous multilayer. Meeting all these requirements is not trivial and a multilayer has to be engineered *ad hoc* for the emissive material under investigation. The configuration implemented in this study, instead, is a device platform suitable for different emitting materials and that enabled easily to test three anthracene derivatives.

Besides the multilayer approach, other strategies can be implemented for improving brightness in OLETs, such as engineering the overall device architecture by means of microlens arrays, microcavity, photonic crystals, nanostructures or surface plasmon enhancing structures for obtaining spectral and out-coupling modulation of the electroluminescence ^[20].

References

- [1] T. Sakanoue, M. Yahiro, C. Adachi, H. Uchiuzou, T. Takahashi, A. Toshimitsu, *Appl. Phys. Lett.* **2007**, *90*, 1.
- [2] T. H. Ke, R. Gehlhaar, C. H. Chen, J. T. Lin, C. C. Wu, C. Adachi, *Appl. Phys. Lett.* **2009**, *94*.
- [3] R. Capelli, S. Toffanin, G. Generali, H. Usta, A. Facchetti, M. Muccini, *Nat. Mater.* **2010**, *9*, 496.
- [4] M. A. McCarthy, B. Liu, E. P. Donoghue, I. Kravchenko, D. Y. Kim, F. So, A. G. Rinzler, *Science.* **2011**, *332*, 570.
- [5] M. Muccini, S. Toffanin, *Organic Light-Emitting Transistors: Towards the Next Generation Display Technology*, Ed. Wiley-Science, Wise Co-Publication, **2016**.
- [6] S. L. Lin, L. H. Chan, R. H. Lee, M. Y. Yen, W. J. Kuo, C. T. Chen, R. J. Jeng, *Adv. Mater.* **2008**, *20*, 3947.
- [7] Y. Zhang, S. L. Lai, Q. X. Tong, M. F. Lo, T. W. Ng, M. Y. Chan, Z. C. Wen, J. He, K. S. Jeff, X. L. Tang, W. M. Liu, C. C. Ko, P. F. Wang, C. S. Lee, *Chem. Mater.* **2012**, *24*, 61.
- [8] S.-H. Lin, F.-I. Wu, H.-Y. Tsai, P.-Y. Chou, H.-H. Chou, C.-H. Cheng, R.-S. Liu, *J. Mater. Chem.* **2011**, *21*, 8122.
- [9] Y. H. Kim, H. C. Jeong, S. H. Kim, K. Yang, S. K. Kwon, *Adv. Funct. Mater.* **2005**, *15*, 1799.
- [10] H. Park, Y.-H. K. Jonghee Lee, II Kang, Hye Yong Chu, Jeong-Ik Lee, Soon-Ki Kwon, *J. Mater. Chem.* **2012**, *22*, 2695.
- [11] R. Kim, S. Lee, K. Kim, Y. Lee, S. Kwon, J. Kim, Y. Kim, *Chem. Commun.* **2013**, *49*, 4664.
- [12] J. Hu, Y. Pu, F. Satoh, S. Kawata, H. Katagiri, *Adv. Funct. Mater.* **2014**, *24*, 2064.
- [13] Y. Fukuda, T. Watanabe, T. Wakimoto, S. Miyaguchi, M. Tsuchida, *Synth. Met.* **2000**, *111-112*, 1.
- [14] Y. Yuan, G. Giri, A. L. Ayzner, A. P. Zoombelt, C. Jihua, M. S. C. B., D. Nordlund, F. T. Michael, J. Huang, Z. Bao, *Nat. Commun.* **2014**, *5*, 3005.
- [15] T. Matsushima, A. S. D. Sandanayaka, Y. Esaki, A. Chihaya, *Sci. Rep.* **2015**, *5*, 14547.
- [16] E. B. Namdas, P. Ledochowitsch, J. D. Yuen, D. Moses, A. J. Heeger, E. B.

- Namdas, P. Ledochowitsch, J. D. Yuen, D. Moses, *Appl. Phys. Lett.* **2008**, *92*, 1.
- [17] J. H. Seo, E. B. Namdas, A. Gutacker, A. J. Heeger, G. C. Bazan, *Adv. Funct. Mater.* **2011**, *21*, 3667.
- [18] Tsung-ChengTsai, Wen-YiHung, Liang-ChenChi, Ken-TsungWong, Cheng-ChihHsieh, Pi-TaiChou, *Org. Electron.* **2009**, *10*, 158.
- [19] S. Toffanin, R. Capelli, W. Koopman, G. Generali, S. Cavallini, A. Stefani, D. Saguatti, G. Ruani, M. Muccini, *Laser Photonics Rev.* **2013**, *7*, 1011.
- [20] K. Saxena, V. K. Jain, D. S. Mehta, *Opt. Mater. (Amst).* **2009**, *32*, 221.

Chapter 5

Integration of multilayer high-k photonic crystal into transparent ambipolar OLET

5.1 Introduction

One of the key problems with OLETs is their low brightness, which limits their application. As already discussed in the previous chapter, the brightness and light emission performance reported for OLETs in the literature are rather low mainly because it is quite difficult to have good carrier transport and high electroluminescence simultaneously in the organic material ^[1]. The multilayer approach showed the highest potential when implementing sublimated small molecules in the device active region ^[2]. However, with molecules combining both ambipolar charge capability and light emitting properties, a single-layer structure based device is highly preferable due to the simpler fabrication process. In these cases, other strategies can be implemented for improving brightness, such as engineering the overall device architecture for optimizing light extraction and out-coupling. Various approaches have been implemented to improve the external coupling of light in OLEDs by means of internal and external device modification techniques such as substrate modification methods, use of scattering media, microlens arrays, microcavity, photonic crystals, nanocavities, nanoparticles, nanowires, nanostructures, and surface plasmon enhancing structures ^[3]. Microcavity is a particular photonic structure able to redistribute the photon density of states such that only certain wavelengths, which correspond to allowed cavity modes, are emitted in a given direction. Planar Distributed Bragg reflectors (DBR) represent an example of

microcavity. Bragg reflectors are multilayer photonic crystal, that is a periodic structure of materials (generally inorganic) with different refractive indices which can create a range of forbidden frequencies called a Photonic Band Gap. Photons with energies lying in the bandgap cannot propagate through the medium. This gives the opportunity to shape and mould the flow of light and thus modulate the device photonic characteristics^{[4][5]}. The introduction of planar microcavities in OLEDs were actively studied for improving performance and was demonstrated to modify the spontaneous emission^{[6][7]}. This approach for modulating the device photonic characteristics can be only partially implemented in the case of OLET planar architecture. Indeed, a vertical microcavity is formed by the substrate-integrated DBR mirror and the metal (reflecting) electrode only when electroluminescence is formed underneath the electrode, i.e. in unipolar bias condition^[8]. In this bias condition, the light formation process is inherently inefficient due to the exciton and light quenching mechanisms correlated to the proximity of the electrode^[9].

Instead of implementing the DBR as a mere optical elements, Namdas et al.^[10] proposed to insert the inorganic multilayer cavity as the gate dielectric in OLET in order to enhance the device brightness in forward direction. The optical thickness of the multilayer dielectric was optimized in order to allow the stack to work as a reflector that enhanced the brightness of the emission from the device.

In addition to the photonic functionality, the optically active dielectric has to fulfill all the standard requirements for the gate dielectric of an OLET. Particularly, it needs to have the following: (i) low gate leakage current; (ii) the ability to sustain high voltage without dielectric breakdown; (iii) low density of electrons traps; (iv) high, or at least moderate, capacitance in order to have reasonable operating voltage; and (v) low surface roughness.

The ambipolar single-layer NT4N-based OLET optimized in this thesis and presented in chapter 3, represents an ideal device platform for the integration of a photonic structure. In order to modulate the electroluminescence signal of the device in direction and intensity, my research activity was focused on realizing a transparent highly-integrated optoelectronic organic device by replacing the PMMA gate dielectric with a transparent multilayer photonic crystal (ML-PhC) comprised by a stack of alternating high-k $\text{ZrO}_2/\text{Al}_2\text{O}_3$ layers with different refractive indices as an optoelectronic gate dielectric.

5.2 Gate dielectric Photonic Crystal

The outperforming device architecture comprised by glass/ITO/PMMA/NT4N/Au with a 75 nm-thick active layer was the starting point to engineer a transparent optoelectronic organic device by introducing a photonic crystal as a multistack gate dielectric. The polymeric dielectric was replaced with a gate dielectric photonic crystal fabricated at the IIT of Milano by Pulsed Laser Deposition (PLD). This technique guarantees the deposition of stacks of homogeneous, low-roughness and dense oxide layers^[11]. The design and characterization of the photonic features of the ML-PhC substrates were performed in collaboration with the Politecnico in Milano. In Figure 5.1 the scheme and the scanning electron microscope (SEM) image of the cross-section of the PhC-OLET fabricated onto glass/ITO substrate in a top contact/bottom gate configuration are reported. The overall dielectric is composed of a stack of 9 alternating high-density layers of ZrO₂ and Al₂O₃ and a 40 nm-thick buffer layer of polymethylmethacrylate (PMMA).

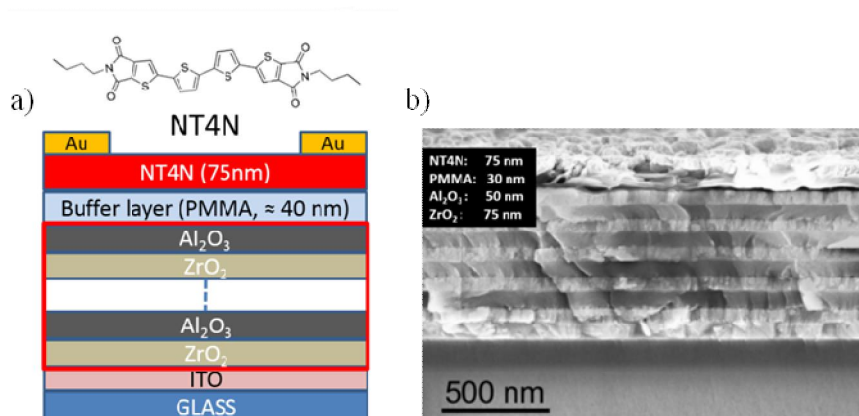


Figure 5.1 (a) Schematics of the PhC-OLET where a ML-PhC is integrated as dielectric in standard top contact/bottom gate device configuration. (b) SEM image of the stack constituting the device active region: the alternating layers of ZrO₂ and Al₂O₃ are reported.

Since preliminary tests showed that even single random surface defects occurred during the multilayer stack growth could affect the electrical insulation of the gate dielectric, a PMMA buffer layer was introduced in order to reduce the intrinsic roughness of the inorganic layer and preserve the usual interface that guarantees the proper packing of NT4T molecules. The thickness of each layer comprising the overall dielectric structure (i.e. ZrO₂, Al₂O₃ and PMMA) was defined by optical simulations according to the

specific requirements on the emission characteristics of the PhC-OLET devices. The band gap of the photonic crystal was designed according to the electroluminescence (EL) spectrum of the NT4N-based OLET. In particular, two different sets of substrate-integrated ML-PhCs were fabricated such that the maximum of the NT4N EL spectrum was located either in correspondence to the minimum of the ML PhC transmittance spectrum (ML-PhC₁ in Figure 5.2 a) or to the maximum of the first-derivative function of the transmittance spectrum (ML-PhC₂ in Figure 5.2 a). In the case of ML-PhC₁, we expected that the ML-PhC works as a DBR reflector thus enabling light reflection at the active layer/dielectric interface towards the direction normal to the glass/ITO substrate (top-view direction) (Figure 5.2 b). In the case of ML-PhC₂, the condition that the derivative of the transmittance is maximized in the proximity of the maximum of the EL spectrum is compatible with an effective modulation of the spectral and spatial distribution of the modes of the emitted light.

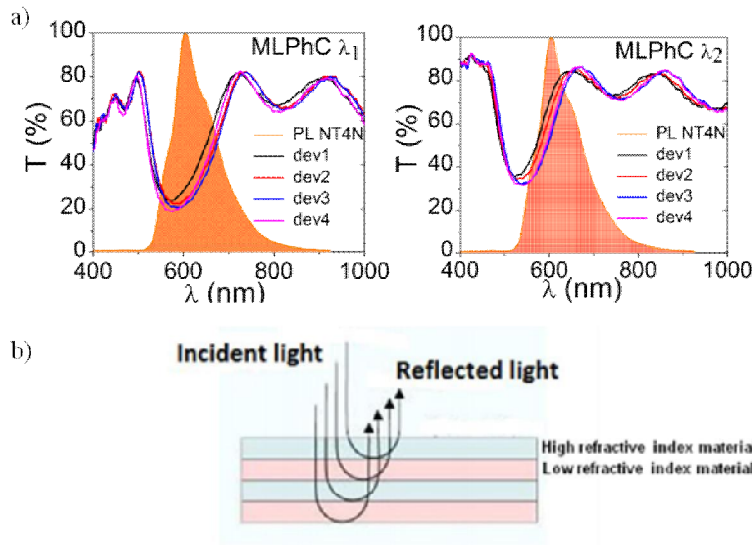


Figure 5.2 (a) Transmittance spectra collected at normal incidence of the stack comprised by Glass/ITO/ML-PhC. (b) Multilayer Photonic Crystal vertical section together with a scheme that shows the behaviour of light in an optical multilayer.

Optical simulations showed that a thickness of PMMA layer equal to 40 nm ensured an unaltered overall spectral responsivity of the photonic crystal (Figure 5.3).

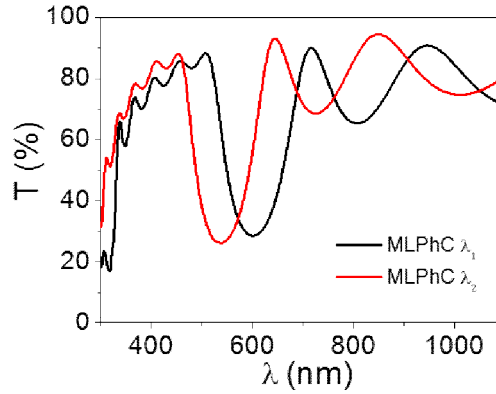


Figure 5.3 MATLAB optical simulations of the multistack vertical structure comprising by glass/ITO/ML-PhC/PMMA named as ML PhC ₁ and ML PhC ₂.

Moreover, this layer thickness allows for depositing a film with low leakage-currents, around 10 nA, and low surface root-mean-square roughness of about 2-3 nm (Figure 5.4).

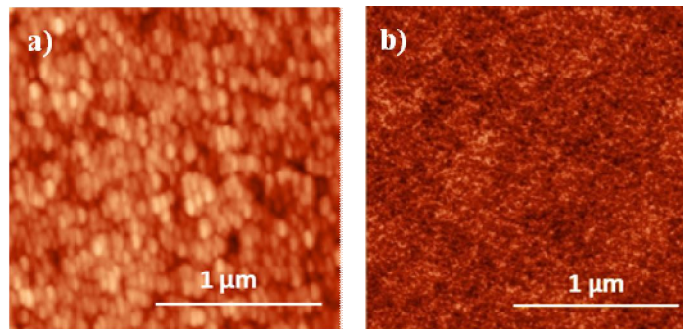


Figure 5.4 Atomic Force Microscope topographical images of the PMMA buffer layer once deposited on top of the multilayer photonic crystal (Roughness RMS: 3 nm) (a) and of the PMMA 450 nm-thick dielectric layer directly deposited onto the ITO/glass substrate (Roughness RMS: 1 nm) (b).

The root-mean-square roughness values of the surfaces of the polymer-functionalized photonic crystal and of the reference 450 nm-thick PMMA layer are similar. The standard requirements for the gate dielectric characteristics in a field-effect transistor are thus fulfilled. Moreover, despite the deposition of a low dielectric-constant organic layer ($k_{\text{PMMA}} \sim 4$), the capacitance of the overall PMMA-functionalized 9-layer ML-PhC was around 20 nF/cm² in the case of the multistack dielectric structures used, which ranged from 580 to 650 nm in thickness according to the specific photonic requirements (ML-

PhC₁ and ML-PhC₂ sets). This capacitance value is more than 2.5 times higher with respect to the capacitance of the 450-nm thick polymeric PMMA dielectric used in reference OLET (i.e. 7.59 ± 0.02 nF/cm²). The overall ML-PhC thickness was found to be constant within a 5% variation over the 3.3 cm²-wide deposited area, as a result of the precise control over each single layer of Al₂O₃ and ZrO₂ comprising the multilayer. Thus, the Photonic Band Gap (PBG) position and width were observed to vary by only 10% throughout the whole area. Transmittance measurements were done in correspondence of the area where the active area of the device would be placed in order to have a control for the specific device.

To compare the performance of the device in this new architecture, the standard single-layer OLETs used as reference were produced in a top contact/bottom gate configuration, using 450 nm of PMMA as dielectric layer. NT4N semiconductor was thermally sublimated onto the glass/ITO/PMMA stacks with a growth rate of 0.6 nm/min. The thickness of the semiconducting layer was 75 nm. These are the growth conditions previously optimized (see Chapter 3) and which guarantee the best optoelectronic performances. Finally, as injecting electrodes 70 nm gold layers were evaporated on top of the semiconductor with a source-drain channel length of $L = 70$ μm and a channel width of $W = 1.2$ cm. Figure 5.5 shows the realized device.



Figure 5.5 Transparent single-layer ambipolar NT4N based OLETs fabricated on glass/ITO/ML-PhC/PMMA substrate.

5.3 Enhancement of optoelectronic performance in PhC-OLET

Standard electrical characterization for transistor devices was performed in nitrogen atmosphere to investigate the charge transport properties of both the Standard and Photonic OLETs. It was demonstrated that the characteristic FET behavior devices using NT4N as active layer is maintained even when implementing the ML-PhC as gate dielectric.

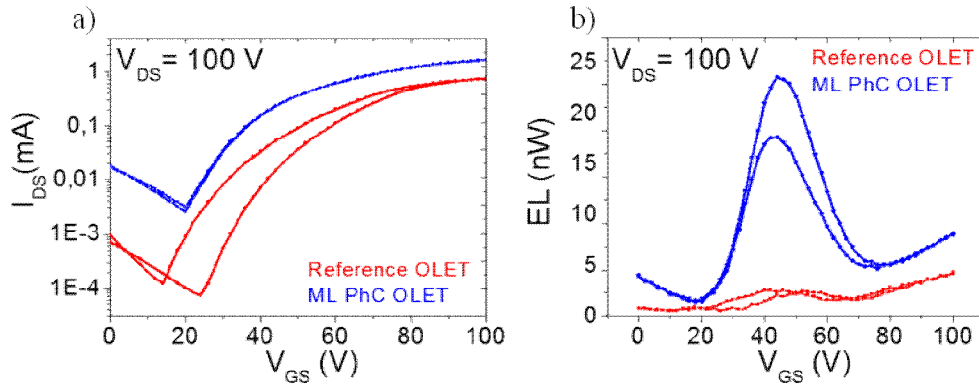


Figure 5.6 (a) n-type saturation transfer characteristic of the PhC-OLET (blue line) compared to the reference OLET (red line) performed by keeping V_{DS} at 100 V. (b) Emitted power curve in bottom direction (through the glass substrate) as a function of the gate voltage during the n-type saturation transfer characteristic reported for the PhC-OLET (blue line) and for the reference OLET (red line). A more-than-6-time factor increase in the emitted power is achieved in the PhC-OLET.

The transfer curves (Figure 5.6 a) exhibit for both Standard and Photonic OLET the characteristic V-shaped dependence that indicates the typical ambipolar transport behavior expected for the NT4N active layer material. The asymmetry is ascribed to unbalanced charge transport and to different voltage absolute threshold values for electrons and holes. Considering the principal electrical parameters extrapolated from the n- and p-type transfer curves which are reported in Table 5.1, the electron mobility (μ_e) is two orders of magnitude higher than the hole mobility (μ_h) in NT4N-based OLETs.

Table 5.1 Comparison of the electrical and optical parameters between the reference and the ML-PhC integrated OLETs.

	μ_e [cm ² /Vs]	μ_h [cm ² /Vs]	I_{DS} Max n- type [mA]	I_{DS} Max p- type [mA]	$V_{t,e}$ [V]	$V_{t,h}$ [V]	Max Emitted Power* [nW]	Brightness *+ [cd/m ²]
PMMA -OLET	7.5E-1	1.2E-3	7.3E-1	1.0E-3	38	-67	4.4 (unipolar)	0.18 (unipolar)
PhC- OLET	2.3E-1	4.7E-3	1.6	1.4E-2	21	-58	24.0 (ambipolar)	1.70 (unipolar)

*data collected in n-type saturation bias condition in bottom configuration

+ the Brightness was acquired by a calibrated spectroradiometer from the bottom side of the device. The Brightness Enhancement Factor (BEF) was measured to be ϵ 9.

The electron gate threshold voltage ($V_{t,e}$) is always lower than hole gate threshold voltage ($V_{t,p}$) either using the functionalized ML-PhC or the single-layer PMMA as gate dielectrics. However, the ambipolar source-drain current is increased by a factor 25 while the maximum source-drain current in unipolar saturation bias conditions ($V_{GS} = V_{DS} = 100$ V) is higher than 1.5 mA once the ML-PhC is introduced as gate dielectric. The I_{DS} hysteresis is strongly suppressed in the case of ML-PhC even though the organic semiconductor is still deposited on top of PMMA layer. The main cause of the enhancement of the source-drain current is the reduction of the gate thresholds for both the charge carrier types. While the hole and the electron mobility ratio is almost invariant with respect to the two different dielectrics, $V_{t,e}$ is reduced by 46% and $V_{t,h}$ by 13% in the case of the PhC-OLET. The gate-threshold reduction is due to the higher capacitance of the PMMA-buffered inorganic multilayer stack. To note that the reduction of $V_{t,h}$ is much less than $V_{t,e}$. The unbalance in the electron and hole gate-threshold voltage clearly affects the shape of the n-type multiple output characteristics reported in Figure 5.7 a: indeed, the I_{DS} vs V_{DS} curves are characterized by a linear region followed by a saturation regime for each V_{GS} value, as it is typically observed for unipolar field-effect transistors. However, EL output characteristics curves (dotted lines in Figure 5.7 a) show indication of ambipolar transport regime: the curves are characterized by a superposition of standard saturation behavior for one charge carrier at high V_{GS} and a superlinear current increase at low V_{GS} and high V_{DS} due to injection of the other charge carrier. In Figure 5.7 b the output characteristics of the reference OLET are reported for comparison.

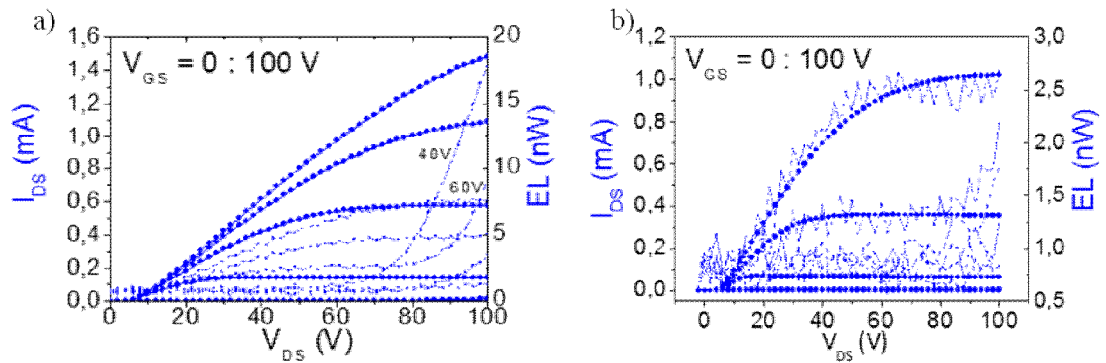


Figure 5.7 Comparison between the multiple output characteristics of the PhC-OLET (a) and the reference (b) OLET: source-drain current (dotted line) and emitted power (squared line) are reported.

As expected, the electroluminescence is peaked in correspondence to the ambipolar region ($V_{GS} \sim 1/2V_{DS}$) where the balance between the hole and electron current is maximized (Figure 5.6 b). The most striking feature is that PhC-OLET presents a more-than-10-times factor increase in the emitted power as compared with the standard OLET when light is collected through the transparent substrate at maximum intensity ($V_{GS} = 40$ V $V_{DS} = 100$ V). Since no considerable signal is collected in the top-view direction in the case of the reference OLET, in order to assess the variation on the OLET optoelectronic performance due to the ML PhC integration, the light-collection configuration through the glass-ITO substrate was preferred. In this bottom-view direction (the ML-PhC₁ dielectric was tailored to reflect the EL in the top-view direction) the increase in the observed emitted power is possibly related to the 25-fold increase in the source-drain current flowing in the device channel in ambipolar bias regime. Indeed, given the lower values of threshold voltage obtained using a high-k dielectric, the current flowing within the device channel is higher in the case of PhC-OLET, as can be clearly seen in Figure 5.6 a. Also the external quantum efficiency (EQE) increases when comparing PhC-OLET and the reference OLET. If we calculate the EQE at the maximum of the optical power for each of the two devices, we obtain a factor 3 increase in the case of case of the PhC-OLET. Moreover, the EQE value reaches as high as 0.027% when the photonic device is driven in real ambipolar bias conditions (at around 20 V): interestingly, the corresponding value for the reference OLET cannot be determined given that the device is still in off condition at voltage biased. Although the EQE observed in ambipolar condition in the case of PhC-OLET is low, probably due to the high current density, it is worth to note that the integration of the photonic crystals

permits to achieve a valuable improvement in respect to the case of PMMA-OLET. The brightness was measured in unipolar conditions with a standard calibrated spectroradiometer in point-like emitting source conditions. To directly compare the PhC-OLET with the PMMA reference, the measurements were performed in unipolar saturation bias condition, since at $V_{DS} = 40V$, while the PhC-OLET presents the maximum of electroluminescence, the light emitted by the PMMA-OLET is too low to permit a reliable measurement. In this condition, a 9-time enhancement in the brightness was observed for the photonic integrated device. Unfortunately the brightness values measured are quite low. It is mainly due to the low quantum yield of the organic active material NT4N in thin film (about 5%) and to the unbalanced charge transport, but it is also important to consider the system used for the brightness measurement. Moreover, it is important to note that, since we aimed to increase both the optical and the electrical properties of the device, the ML-PhC was fabricated as thin as possible in order to obtain a good capacitance. As a consequence, with the used materials it was possible to obtain a maximum reflectivity of about 60% that represents the most effective trade-off between the minimization of the overall dielectric thickness and the maximization of the number of the layers of the ML-PhC.

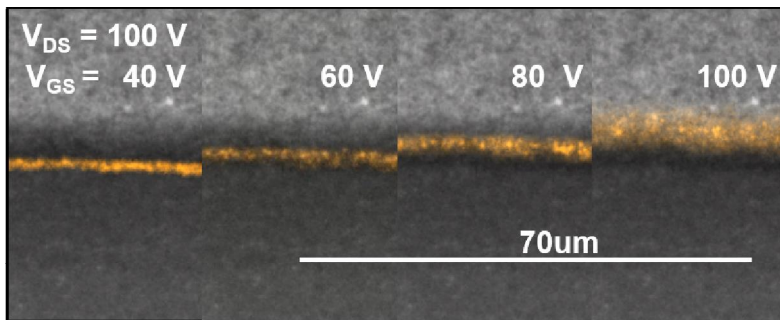


Figure 5.8 Microphotographs of the emission zone locations within the channel of the PhC-OLET as the source-gate voltage is varied from 40 V to 100 V while keeping the source-drain voltage constant at 100V.

It can be observed that in ambipolar bias condition ($V_{GS} = 40 V$ and $V_{DS} = 100 V$) the emission stripe is about μm -away from the drain electrode.

As a fingerprint of the ambipolar charge transport, we observed the expected gate-voltage dependent location of the emission zone in the channel of the ML-PhC OLET from microns-away distance to underneath the drain electrode (Figure 5.8)

5.4 Modulation of optical characteristics in PhC-OLET

Differently from the other reported photonics-integrated OLETs^{[11][12]}, the full transparency of the device substrate allows us to probe directly the optical characteristics of the EL emitted both through the glass-ITO substrate (bottom view direction) and at the organic semiconductor/atmosphere interface (top view direction). In order to perform the optical characterization onto an optical bench, the PhC-OLET device chip was encapsulated: the light extracted in top view direction passes through a 350 μm -thick N_2 layer and a 1 mm-thick glass cap before escaping. The devices were encapsulated in the glovebox using a glass coverslip and an ultraviolet-cured epoxy sealant. Figure 5.9 a, shows the modulation of the normalized EL spectra collected in bottom view direction as a function of the photonic band gap of the two different ML-PhC sets. As the photonic band gap is shifted towards lower energy values, the NT4N EL spectrum profile is modulated accordingly. In the case of ML PhC₁ the EL spectrum of NT4N broadens in the full-width-at-the-half-maximum (FWHM) given the increase in intensity of the maximum peak shoulder at 650 nm. In the case of ML PhC₂ the portion of the spectrum at high energy is partially suppressed while a new maximum peak at 650 nm is present. When using ML-PhC₁, the enhancement of the EL intensity along the optical axis in the top view direction is expected given that it was designed as a DBR. Figure 5.9 b reports the experimental EL spectra of the PhC-OLET based on ML-PhC₁ collected along the optical axis in the top and bottom view directions. The corresponding simulated spectra obtained by means of a commercial optoelectronic simulation software (FLUXiM-Setfos)^[13] are also reported. According to the simulations, a higher intensity (of about a 4-fold factor) is expected when EL is collected along the optical axis in top view. This evidence was corroborated by the experimental measurements as reported in Figure 5.9 b.

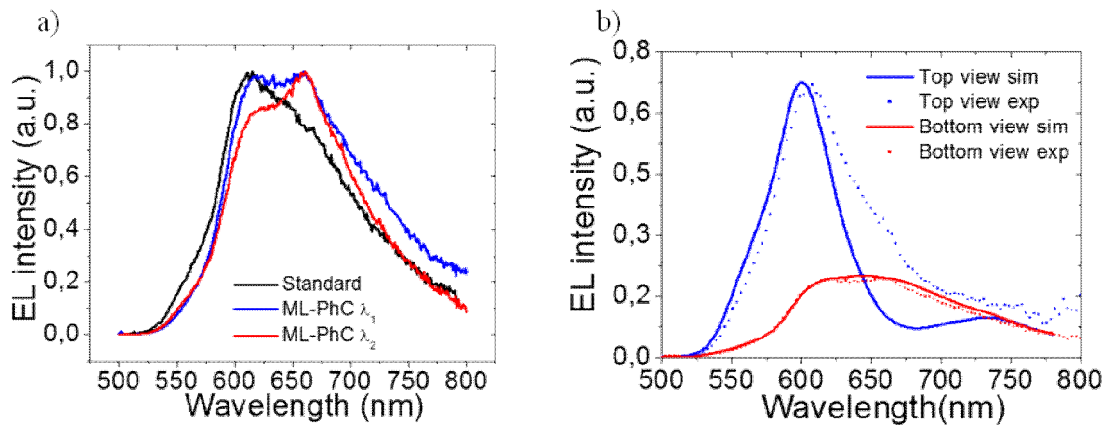


Figure 5.9 (a) Modulation of the EL spectra from bottom view with respect to reference NT4N-based OLET (black line) by introducing ML-PhCs with different PBGs (blue and red lines) as ML-PhC dielectric in OLET structure. (b) Comparison between the EL spectra of PhC-OLET (ML-PhC λ_1) collected along the optical axis in the top view (blue squares) and in the bottom view (red squares) directions. In solid line the corresponding simulated spectra. The relative intensity of the top-view and bottom-view spectra is real (both experimental and simulated). The spectra are collected in ambipolar bias conditions.

However, the experimental spectral profile in top-view at higher wavelengths is only partially in accordance with the simulated one possibly due to software approximations. Indeed, as the SEM image shows in Figure 5.1 b, the NT4N thin-film is not a compact and homogenous layer, rather an arrangement of three-dimensional slab-like crystalline domains that may contribute to light scattering phenomena which are not accounted for in the simulations. In order to probe efficiently the modulation of the spatial distribution of the emitted light due to the integration of the ML-PhC in the proximity of the charge recombination region of the device, we collected angular EL in ambipolar bias conditions profiles by rotating the device optical axis with respect to the light collection direction in bottom-view. In the case of the reference OLET (Figure 5.10 a, dotted line), the angular profile is almost Lambertian as already reported in literature in the case of a device in top-contact bottom-gate configuration with a multilayer stack as active region^[14]. Instead, the pattern of emitted photons is modified with the integration of the ML-PhC (specifically ML-PhC λ_1 in Figure 5.10 b, dotted line). The angular emission profile becomes broader with a maximum at 40°-60°. The error distribution for the reported emission profile measurements is below 1%. The good accordance of the experimental data with the emission patterns simulated by FLUXiM-Setfos (Figures 5.10 a and b, solid lines) confirms that the photonic multilayer structure is responsible

for the modulation of the spatial distribution of the emitted photons. The PhC-OLET device in ambipolar regime is simulated by a multistack structure formed by a glass/ITO/ML-PhC/PMMA substrate and the NT4N organic stack. Then, we introduced a gold layer on top of the structure in order to simulate the light outcoupling in unipolar bias conditions: no correspondence with the experimental data was observed. Moreover, no modulation of the collected angular profiles is observed when modulating the gate voltage from ambipolar to unipolar bias conditions. Although the emission zone clearly shifts to the proximity of the electrode as the gate voltage increases (Figure 5.8), no effective microcavity between the DBR and the gold electrode is formed. This emitted-photon pattern is different from what reported in literature for other OLETs integrated with photonic components given that the EL features were strongly modulated by the microcavity in unipolar transistor reported by Hu et al. ^{[8][15]}. The absence of unwanted microcavity effects in the case of NT4N-based PhC-OLET may be correlated to the particular morphology of the metal/organic interface in top-contact device configuration, which in turn is expected to alter the reflectivity properties of the gold electrode. As it can be seen in the SEM image in Figure 5.11, the interface between the organic semiconductor and the injecting electrode is inhomogeneous, not continuous and grain-like with evident diffusion of the metal nanostructures within the active layer.

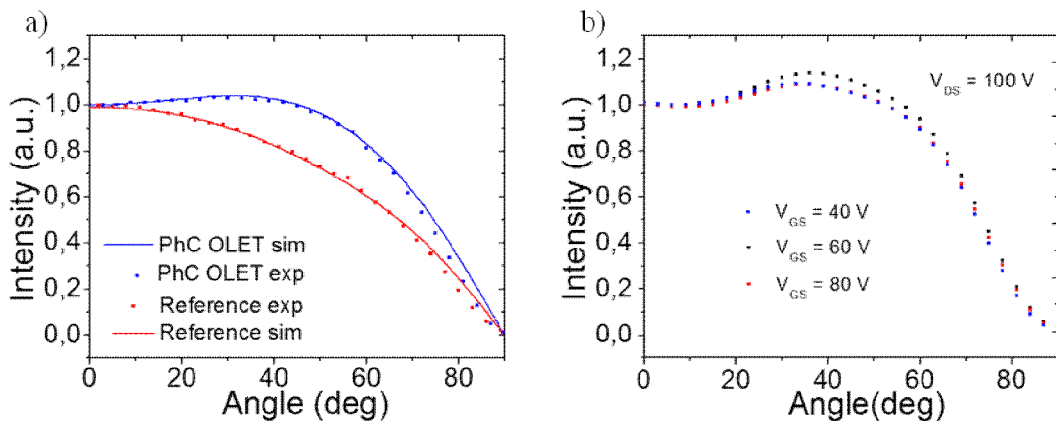


Figure 5.10 (a) Measured (squares) and simulated (solid line) EL intensity angular profiles collected through the glass-ITO substrate in ambipolar bias conditions for reference OLET (red line) and PhC-OLET with ML-PhC₁ (blue line) as dielectric. (b) Comparison between EL intensity angular profiles collected through the glass-ITO substrate by varying V_{GS} from 40 to 100 V while keeping V_{DS} at 100 V.

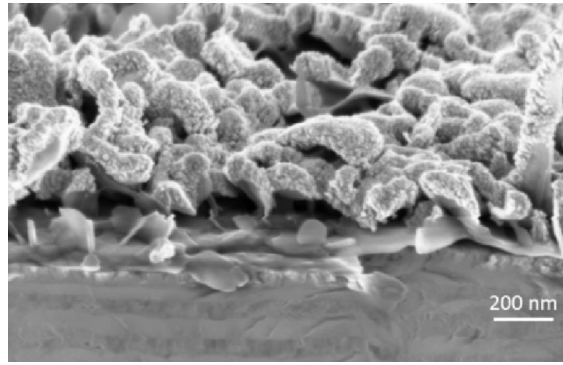


Figure 5.11 SEM image of the stack comprising the PMMA-functionalized ML PhC, the NT4N active layer and the gold injecting electrode.

5.5 Conclusions

In order to modulate and enhance the photonic properties in OLET devices, my work was focused on engineering a transparent highly-integrated optoelectronic organic device by introducing a one-dimensional photonic crystal as a multistack gate dielectric. By achieving the most effective trade-off between high capacitance and good reflectivity, the integrated photonic structure is not only capable of modulating the optical characteristics of the emitted light but also of improving the electrical performance of the devices. Indeed, the use of a ML-PhC comprised by high-k materials (alternated layer of Al_2O_3 and ZrO_2) as gate dielectric allows to reduce the threshold voltage and to improve the source-drain current in ambipolar bias conditions with respect to the reference device based on polymeric dielectric. The transparency of the substrate, contrary to the more often used conducting silicon wafer^[10], enables light collection both in the top and bottom-view directions. In the latter case the brightness and optical power are both increased with respect to the reference PMMA-OLET as a consequence of the higher current density flowing in the device. By fine-tuning the position and the width of the photonic band gap of the ML-PhCs with respect to the electroluminescence spectrum of the organic active layer, it was possible to tune the optical features of the OLET emitted light. In this specific case, the overall thickness of the structure (and thus the thickness of each layer comprising it) was engineered in order to realize a DBR. By controlling the location of the emission zone inside the channel region, the OLET brightness was increased by more than 4 time factor in ambipolar condition when light is collected in the top-view direction, demonstrating that the

$\text{Al}_2\text{O}_3/\text{ZrO}_2$ multilayer acts as a DBR, as expected from the optical simulation. Furthermore, the integration of the ML-PhC induces a photonic effect, modifying the EL spectrum profile and modulating the angular profile from the Lambertian behaviour.

The integration of planar DBRs into the active region of efficient OLETs is a possible route for realizing the long-sought-for electrically-pumped organic laser ^[14]. As a further development, an organic Vertical Cavity Surface Emitting Laser may be realized by sandwiching the active channel of the OLET as the gain medium between two DBRs based on ML-PhCs.

References

- [1] M. Muccini, S. Toffanin, *Organic Light-Emitting Transistors: Towards the Next Generation Display Technology*, Ed. Wiley-Science, Wise Co-Publication, **2016**.
- [2] R. Capelli, S. Toffanin, G. Generali, H. Usta, A. Facchetti, M. Muccini, *Nat. Mater.* **2010**, *9*, 496.
- [3] K. Saxena, V. K. Jain, D. S. Mehta, *Opt. Mater. (Amst)*. **2009**, *32*, 221.
- [4] K. Sakoda, *Optical Properties of Photonic Crystals*, Springer, Berlin, **2005**.
- [5] J. J. D., P. R. Villeneuve, S. Fan, *Nature* **1997**, *386*, 143.
- [6] A. Dodabalapur, L. J. Rothberg, T. M. Miller, E. W. Kwock, *Appl. Phys. Lett.* **1994**, *64*, 2486.
- [7] W. C. H. Choy, C. Y. Ho, *Opt. Express* **2007**, *15*, 13288.
- [8] Y. Hu, J. Lin, L. Song, Q. Lu, W. Zhu, X. Liu, *Nat. Publ. Gr.* **2016**, *1*.
- [9] M. Muccini, W. Koopman, S. Toffanin, *Laser Photonics Rev.* **2012**, *6*, 258.
- [10] E. B. Namdas, B. B. Y. Hsu, J. D. Yuen, I. D. W. Samuel, A. J. Heeger, *Adv. Mater.* **2011**, *23*, 2353.
- [11] L. Passoni, L. Criante, F. Fumagalli, F. Scotognella, G. Lanzani, F. Di Fonzo, N. Science, T. Polimi, I. Italiano, V. G. Pascoli, D. Fisica, *ACS Nano* **2014**, 12167.
- [12] B. M. C. Gwinner, S. Khodabakhsh, M. H. Song, H. Schweizer, H. Giessen, H. Sirringhaus, *Adv. Funct. Mater.* **2009**, *19*, 1360.
- [13] B. Perucco, N. A. Reinke, D. Rezzonico, M. Moos, B. Ruhstaller, *Opt. Express* **2010**, *18*, 246.
- [14] S. Toffanin, R. Capelli, W. Koopman, G. Generali, S. Cavallini, A. Stefani, D. Saguatti, G. Ruani, M. Muccini, *Laser Photonics Rev.* **2013**, *7*, 1011.
- [15] Y. Hu, L. Song, D. Li, J. Lin, X. Liu, *Org. Electron.* **2015**, *26*, 92.

Conclusions

Organic light-emitting field-effect transistors (OLETs) are emerging as an innovative class of multifunctional devices that integrates the electronic properties of a transistor, the light generation capability and the full potential of organic photonics.

In the scientific work reported in this thesis we deal with the engineering of the different constituting elements of OLETs in order to optimize and improve the technology-relevant figures of merit of this device platform. In particular, we focus our attention on the design, implementation and validation of effective processing protocols and innovative architectures of the active-material region and of the gate dielectric within OLETs.

The optoelectronic figures of merits of field-effect devices based on organic thin-films, such as field-effect mobility and light emission in the case of OLETs, are indeed deeply connected to both the organic semiconductors characteristics (i.e. molecular structure, packing adopted in the solid state and thin-film morphology) and to the device configuration and architecture. Firstly, we investigated the strict correlation between the structural arrangements in solid state and the optoelectronic performance in NT4N-based thin-films by implementing different deposition techniques for fabricating the device active layer. The NT4N multifunctional small-molecule organic semiconductor is an oligothiophene derivative bearing 2,3-thienoimide symmetric ends, recently synthesized and studied at CNR-ISOF in Bologna, which shows ambipolar charge transport and electroluminescent properties. Interestingly, as many other organic linear conjugated compounds, it presents different polymorphic phases in solid-state. In order to investigate how the possible different molecular arrangements may modulate the optoelectronic device performance, we fabricated thin-film field-effect transistors based on NT4N by using thermal sublimation, Supersonic Molecular Beam Deposition (SuMBD) and Lithographically Controlled Wetting (LCW). In addition to the two polymorphs already reported in literature, a third supramolecular arrangement was discovered by using a specific deposition technique (i.e. SuMBD), together with the corresponding optimized recipe. Moreover, comparing electrical characteristics of devices fabricated by two different dry deposition techniques (thermal sublimation vs SuMBD), we observed that different morphological features in the deposited thin-films are evidently correlated to different charge-carrier mobility even though the crystalline

phase remains invariant. Finally, the use of liquid method as LCW allowed us to obtain dense nanopatterned fiber-based thin-film that enabled for the first time field-effect charge transport behaviour in NT4N based organic field-effect transistors once realized by wet technique.

Although the use of a single ambipolar electroluminescent active layer in OLETs represents one of the most challenging and intriguing approaches for realizing devices, it requires a material capable of both high charge mobility in field-effect charge transport configuration and efficient light emission. Since these features often are self-excluding in the solid state in conjugated organic compounds, the implementation of a multilayer architecture represents a suitable way to optimize each functionalities (i.e. hole/electron transport, charge recombination, light emission) independently. In collaboration with the CNR-ISOF in Bologna, a new anthracene-based compound, namely DiPAXA was synthesized according to the structure-design requirements proposed in literature for obtaining deep-blue emitting materials. The requirement of π -conjugation extent reduction in order to prevent red-shifted emission and strong crystallization usually leads to a poor field-effect mobility. The implementation of a bilayer heterostructure comprising a charge-transport layer and a light-emitting layer, enabled to overcome this problem and separately optimize the emissive layer. In this way a deep blue electroluminescence (color coordinate $x = 0.18$ and $y = 0.21$) close to the standard request and an external quantum efficiency of 0.125 % were obtained.

Instead of using a multilayer approach in realizing the device active region, an effective enhancement in OLET optoelectronic performance (in terms of both brightness and spectral/spatial tunability of the emitted light) can be achieved by integrating a hybrid photonic structure as gate dielectric in the device architecture. Indeed, we introduced a one-dimensional photonic crystal as gate dielectric in the ambipolar single-layer NT4N based OLET that we had previously optimized. The PMMA dielectric was replaced by a multilayer photonic crystal comprised by a stack of alternating high- k ZrO_2/Al_2O_3 layers with different refractive indices engineered in collaboration with the IIT in Milano. By optimizing the thickness and tuning the position of the photonic band gap of the multilayer photonic crystals with respect to the electroluminescence spectrum of the organic active layer, it was possible both to improve the optoelectronic performance and to tune the optical features of the OLET emitted light. A substantial reduction in the threshold voltage and an improvement by a factor 25 of the source-drain current in

ambipolar bias condition was observed. Moreover, we succeed in obtaining an OLET single-layer NT4N-based with brightness 10×higher respect the corresponding standard OLET polymeric dielectric.

Collectively, the experimental evidences reported in this thesis showed that suitable strategies in engineering the single components comprising the OLET device structures surely enable to optimize the light-emission efficiency and brightness of OLETs. These expected improvements as well as the OLET full compatibility with well-established electronic and photonic planar technologies, may allow the development of optical communication systems, integrated optoelectronic systems and electrically pumped organic lasers.

List of publications

M. Natali, S. D. Quiroga, L. Passoni, L. Criante, E. Benvenuti, G. Bolognini, L. Favaretto, M. Melucci, M. Muccini, F. Scotognella, F. Di Fonzo, S. Toffanin, *Simultaneous 10-fold brightness enhancement and emitted-light spectral tunability in transparent ambipolar organic light-emitting transistor by integration of high-k photonic crystal*, Advanced Functional Materials. Accepted for publication.

M. Zambianchi, E. Benvenuti, C. Bettini, C. Zanardi, R. Seeber, D. Gentili, M. Cavallini, M. Muccini, V. Biondo, C. Soldano, G. Generali, S. Toffanin, M. Melucci, *Anthracene-based molecular emitters for non-doped deep-blue organic light emitting transistors*, J. Mater.Chem. C, Vol 4, n. 40, 9411-9417, 2016.

N. Lago, A. Cester, N. Wrachien, E. Benvenuti, S. D. Quiroga, M. Natali, S. Toffanin, M. Muccini, G. Meneghesso, *Investigation of Mobility Transient on Organic Transistor by Means of DLTS Technique*, IEEE Transactions on Electron Devices, Vol. 63, n. 11, p. 4432-4439, 2016.

N. Lago, A. Cester, N. Wrachien, M. Natali, S. D. Quiroga, S. Bonetti, M. Barbato, A. Rizzo, E. Benvenuti, V. Benfenati, M. Muccini, S. Toffanin, G. Meneghesso, *A physical-based equivalent circuit model for an organic/electrolyte interface*, Organic Electronics, Vol. 35, p. 176-185; August 2016.

N. Lago, A. Cester, N. Wrachien, I. Tomasino, S. Toffanin, S.D. Quiroga, E. Benvenuti, M. Natali, M. Muccini, G. Meneghesso, *On the Pulsed and Transient characterization of Organic Field-Effect Transistors*, IEEE Electron Device Letters, Vol. 36, n. 12, 2015.

Acknowledgements

I would like to thank my university supervisor Prof. Alberto Credi and my CNR-ISMN supervisors Dr. Stefano Toffanin and Dr. Michele Muccini.

I would like to thank all the people involved in this work: Manuela Melucci, Massimo Zambianchi, Laura Favaretto and Cristian Bettini of CNR-ISOF, Viviana Biondo, Caterina Soldano, Gianluca Generali, Guido Turatti, Riccardo DeAlpaos and Andrea Stefani of E.T.C. srl, Fabio Di Fonzo and Luigino Criante of IIT-CNST of Milano, Francesco Scotognella of the Politecnico of Milano, Mario Barra and Fabio Chiarella of CNR-SPIN of Napoli, Luana Persano of CNR-Nano of Lecce, Lucia Maini and Chiara Cappuccino of the University of Bologna and Denis Gentili of CNR-ISMN of Bologna.

I would like to thank both my colleagues at CNR-ISMN Santiago, Marco, Federico, Vincenzo, Sergio, Edoardo, Giovanni, Alessandra, Rafael and Giovanna.

I would especially like to thank Caterina Soldano and Viviana Biondo for having taught me how to fabricate a device by thermal sublimation in high vacuum and Vincenzo Ragona for his fundamental technical assistance.